

Probing Majorana Neutrino Textures at DUNE

Kalpana Bora,^{1,*} Debasish Borah,^{2,†} and Debajyoti Dutta^{3,4,‡}

¹*Department of Physics, Gauhati University, Guwahati, Assam 781014, India*

²*Department of Physics, Indian Institute of Technology Guwahati, Assam 781039, India*

³*Harish-Chandra Research Institute,*

Chhatnag Road, Jhansi, Allahabad 211019, India

⁴*Homi Bhabha National Institute, Training School Complex,*

Anushaktinagar, Mumbai - 400094, India

Abstract

We study the possibility of probing different texture zero neutrino mass matrices at long baseline neutrino experiment DUNE particularly focusing on its sensitivity to the octant of atmospheric mixing angle θ_{23} and leptonic Dirac CP phase δ_{cp} . Assuming a diagonal charged lepton basis and Majorana nature of light neutrinos, we first classify the possible light neutrino mass matrices with one and two texture zeros and then numerically evaluate the parameter space which satisfies the texture zero conditions. Apart from using the latest global fit 3σ values of neutrino oscillation parameters, we also use the latest bound on the sum of absolute neutrino masses ($\sum_i |m_i|$) from the Planck mission data and the updated bound on effective neutrino mass M_{ee} from neutrinoless double beta decay ($0\nu\beta\beta$) experiment to find the allowed Majorana texture zero mass matrices. For the allowed texture zero mass matrices from all these constraints, we then feed the corresponding light neutrino parameter values satisfying the texture zero conditions into the numerical analysis in order to study the capability of DUNE to allow/exclude them once it starts taking data. We find that the DUNE will be able to exclude some of these texture zero mass matrices which restrict the $(\theta_{23} - \delta_{\text{cp}})$ to a very specific range of values, depending on the values of the parameters that Nature has chosen.

PACS numbers: 14.60.Pq, 11.10.Gh, 11.10.Hi

* kalpana.bora@gmail.com

† dborah@iitg.ernet.in

‡ debajyotidutta@hri.res.in

I. INTRODUCTION

Since the discovery of the Higgs boson in 2012, the large hadron collider (LHC) experiment has been confirming the validity of the standard model (SM) of particle physics again and again without any convincing signature of new physics beyond the standard model (BSM) till date. In spite of such null results, there are plenty of reasons: both theoretical and observational, which undoubtedly suggest the presence of BSM physics. Observation of tiny but non-zero neutrino masses and large leptonic mixing by neutrino oscillation experiments [1–7] is one such reason that has led to a large number of BSM proposals in the last few decades. The current status of neutrino oscillation experiments can be summarised in terms of 3σ global fit values of neutrino parameters shown in table I.

Parameters	Normal Hierarchy (NH)	Inverted Hierarchy (IH)
$\frac{\Delta m_{21}^2}{10^{-5}\text{eV}^2}$	7.03 – 8.09	7.02 – 8.09
$\frac{ \Delta m_{3l}^2 }{10^{-3}\text{eV}^2}$	2.407 – 2.643	2.399 – 2.635
$\sin^2 \theta_{12}$	0.271 – 0.345	0.271 – 0.345
$\sin^2 \theta_{23}$	0.385 – 0.635	0.393 – 0.640
$\sin^2 \theta_{13}$	0.01934 – 0.02392	0.01953 – 0.02408
δ	$0^\circ - 360^\circ$	$145^\circ - 390^\circ$

TABLE I. Global fit 3σ values of neutrino oscillation parameters [8]. Here $\Delta m_{3l}^2 \equiv \Delta m_{31}^2$ for NH and $\Delta m_{3l}^2 \equiv \Delta m_{32}^2$ for IH.

where NH and IH refer to normal and inverted hierarchical neutrino masses respectively. The above data also allow the possibility of quasi-degenerate neutrinos ($m_1 \approx m_2 \approx m_3$). Although the question of the absolute mass scale of neutrinos remain open at oscillation experiments, cosmology and neutrinoless double beta decay ($0\nu\beta\beta$) experiments put an upper bound on the lightest neutrino mass. For example, the latest Planck experiment data constrain the sum of absolute neutrino masses as $\sum_i |m_i| < 0.17$ eV [9]. Similarly, constraints from the ongoing $0\nu\beta\beta$ experiments [10–13] rule out light neutrino masses around 0.1 eV and above. On the other hand, the leptonic Dirac CP phase δ_{cp} remains undetermined as of now, though a recent hint towards $\delta_{\text{cp}} \approx -\pi/2$ [14] appeared recently from the T2K collaboration.

If neutrinos are Majorana fermions, then two Majorana CP phases come into the picture which however, do not affect neutrino oscillation probabilities, but can be probed at $0\nu\beta\beta$ experiments.

In the three flavour neutrino oscillation scenario, the oscillations are driven by the two mass square differences Δm_{21}^2 and $|\Delta m_{31}^2|$. Out of the three mixing angles, θ_{12} , θ_{13} and θ_{23} governing the oscillation amplitudes, θ_{12} and θ_{13} are very precisely measured. Although the atmospheric mixing angle θ_{23} was measured in 1998 at Super-Kamiokande atmospheric neutrino experiment, yet it is not confirmed if $\theta_{23} = 45^\circ$ i.e. maximal or not. If not, then it may lie either in the higher octant (HO) ($\theta_{23} > 45^\circ$) or in the lower octant (LO) ($\theta_{23} < 45^\circ$). The preliminary results from the T2K experiment [3, 14] prefers near maximal mixing [15] while MINOS [7, 16] and Super-Kamiokande (SK) disfavour maximal mixing [17]. All the global fit analyses are inconsistent with maximal θ_{23} at less than 1σ [8, 18]. Recent NO ν A data exclude the maximal mixing scenario at 2.5σ C.L. [19] favouring the case of two degenerate solutions. So in the present scenario, we have to wait for the long baseline (LBL) accelerator experiments to resolve this ambiguity as well as to measure θ_{23} precisely. The capability of DUNE (Deep Underground Neutrino Experiment) [20–23], NO ν A [24, 25], T2K etc to resolve octant ambiguity has been studied in [26–28]. Octant sensitivity at DUNE in conjunction with reactor experiments is studied in [29, 30]. These long baseline accelerator experiments are sensitive to both $\nu_\mu \rightarrow \nu_e$ (appearance) and $\nu_\mu \rightarrow \nu_\mu$ (disappearance) and synergy between them can enhance the octant sensitivity [31–33]. On the other hand, any terrestrial baseline of several hundred kilometres is sensitive to matter effects. So these LBL experiments, being sensitive to matter effects can discriminate between the two hierarchies [20, 34].

After the precise measurement of θ_{13} , now the whole neutrino community is focusing on the leptonic Dirac CP phase δ_{cp} , which is the only unknown parameter in the three flavour oscillation framework. Although in the quark sector, CP violation is observed and can be explained due to complex Yukawa couplings or complex Higgs field vacuum expectation values [35, 36], it is yet to be discovered in the leptonic sector with some significant degree of precision. The LBL accelerator experiments which are sensitive to $\nu_\mu \rightarrow \nu_e$ channel can probe CP violation in the leptonic sector [20]. From this point of view, the DUNE at Fermilab, the U.S. is the best candidate which will start taking data from next decade. In the literature, recent studies related to CP violation discovery potential of DUNE as well as

other super-beam experiments can be found [37–41].

Before the neutrino oscillation experiments completely remove the existing ambiguities in neutrino parameters like the octant of θ_{23} , Dirac CP phase as well as mass hierarchy at ongoing and near future facilities, it is important to study the predictions for these neutrino observables within different BSM frameworks. Depending on the predictions for such neutrino observables, one can discriminate between different BSM scenarios at the oscillation experiments. However, generic BSM frameworks come with several free parameters, making it difficult to have a robust prediction for a particular neutrino parameter. Reducing the number of free parameters can therefore lead to robust testable predictions of neutrino observables. Such reduction of free parameters can be possible within the framework of flavour symmetry models where the additional discrete or continuous symmetries either relate two or more terms or forbid some terms in the mass matrix. One such possibility arises within the context of texture zeros in leptonic mass matrices. For a complete survey of such texture zeros in lepton mass matrices, please refer to [42]. Different possible flavour symmetric interpretations for the origin of such texture zero mass matrices can be found in [43–52] within the framework of different seesaw models. Such texture zero mass matrices in general, have specific predictions for neutrino oscillation parameters, the consequences of which can be studied from cosmology as well as oscillation experiments point of view. In the light of neutrino oscillation experiment data, one-zero and two-zero texture mass matrices were studied in [53–56] and [52, 57–69] respectively. These texture zero mass matrices were also studied from the perspective of baryogenesis through leptogenesis in [70–76].

In this work, we do a phenomenological study of one-zero and two-zero texture mass matrices assuming the neutrinos to be of Majorana nature and the charged lepton mass matrix to be diagonal. The main motive of this work is two fold. Firstly, we intend to find out the allowed texture zero mass matrices from the requirement of satisfying the latest neutrino oscillation data as well as the cosmological bound on the sum of absolute neutrino masses from the latest Planck mission data [9] and the bound on effective neutrino mass M_{ee} from the latest experimental lower bound on neutrinoless double beta decay half-life [12, 13]. The second objective is to find if any of these textures which are allowed from all experimental constraints can be probed, focusing on the sensitivity of neutrino oscillation experiments like DUNE to the values of θ_{23}, δ_{cp} predicted by a particular texture zero mass matrix. We first numerically determine the values of θ_{23}, δ_{cp} along with other neutrino

parameters which satisfy a particular texture zero condition and then use them in GLoBES software [77, 78] to determine the corresponding experimental sensitivity. We show that these textures can be excluded for some combinations of θ_{23} and δ_{cp} at DUNE. If Nature chooses some values of θ_{23} and δ_{cp} , then how DUNE can allow/exclude a particular mass matrix texture is the goal of this present study. We have found that the two-zero textures are very interesting as DUNE can constrain the $\theta_{23} - \delta_{\text{cp}}$ parameter space more tightly compared to the one-zero textures. We have observed that if Nature prefers normal (inverted) mass ordering, then DUNE can constrain a particular type of texture mass matrix denoted as B1 (B1 and B2) more tightly than any other textures.

This article is organised as follows. In section II, we discuss about the different possible texture zero mass matrices. A brief discussion on DUNE is presented in section III. Section IV contains the details of our numerical analysis while in section V we present our results and discussions. Concluding remarks are given in section VI.

II. TEXTURE ZEROS IN MAJORANA NEUTRINO MASS MATRIX

If light neutrinos are of Majorana nature, the 3×3 mass matrix M_ν is complex symmetric having six independent complex parameters. In such a scenario, the total number of structurally different Majorana neutrino mass matrices with k texture zeros is given by

$${}^6C_k = \frac{6!}{k!(6-k)!} \quad (1)$$

A symmetric mass matrix with more than three texture zeros is not compatible with the observed leptonic mixing and masses. The Pontecorvo-Maki-Nakagawa-Sakata (PMNS) leptonic mixing matrix is related to the diagonalising matrices of charged lepton and neutrino mass matrices as

$$U_{\text{PMNS}} = U_l^\dagger U_\nu \quad (2)$$

In the diagonal charged lepton basis, U_{PMNS} is same as the diagonalising matrix U_ν of the neutrino mass matrix M_ν . In this basis, it was shown [79] that a symmetric Majorana neutrino mass matrix with 3 texture zeros is not compatible with neutrino oscillation data. This leaves us with the possible one-zero and two-zero texture mass matrices. Going by the counting formula mentioned above (1), we can have six possible one-zero texture and fifteen

possible two-zero texture mass matrices. The one-zero texture mass matrices can be written as

$$\begin{aligned}
G_1 : \begin{pmatrix} 0 & \times & \times \\ \times & \times & \times \\ \times & \times & \times \end{pmatrix}, G_2 : \begin{pmatrix} \times & 0 & \times \\ 0 & \times & \times \\ \times & \times & \times \end{pmatrix}, G_3 : \begin{pmatrix} \times & \times & 0 \\ \times & \times & \times \\ 0 & \times & \times \end{pmatrix}, G_4 : \begin{pmatrix} \times & \times & \times \\ \times & 0 & \times \\ \times & \times & \times \end{pmatrix}, \\
G_5 : \begin{pmatrix} \times & \times & \times \\ \times & \times & 0 \\ \times & 0 & \times \end{pmatrix}, G_6 : \begin{pmatrix} \times & \times & \times \\ \times & \times & \times \\ \times & \times & 0 \end{pmatrix}
\end{aligned} \tag{3}$$

Where the crosses “ \times ” denote non-zero arbitrary elements of M_ν . Similarly, the two-zero texture matrices, classified into six categories (following the notations of [65]) are given by

$$A_1 : \begin{pmatrix} 0 & 0 & \times \\ 0 & \times & \times \\ \times & \times & \times \end{pmatrix}, A_2 : \begin{pmatrix} 0 & \times & 0 \\ \times & \times & \times \\ 0 & \times & \times \end{pmatrix}; \tag{4}$$

$$B_1 : \begin{pmatrix} \times & \times & 0 \\ \times & 0 & \times \\ 0 & \times & \times \end{pmatrix}, B_2 : \begin{pmatrix} \times & 0 & \times \\ 0 & \times & \times \\ \times & \times & 0 \end{pmatrix}, B_3 : \begin{pmatrix} \times & 0 & \times \\ 0 & 0 & \times \\ \times & \times & \times \end{pmatrix}, B_4 : \begin{pmatrix} \times & \times & 0 \\ \times & \times & \times \\ 0 & \times & 0 \end{pmatrix}; \tag{5}$$

$$C : \begin{pmatrix} \times & \times & \times \\ \times & 0 & \times \\ \times & \times & 0 \end{pmatrix}; \tag{6}$$

$$D_1 : \begin{pmatrix} \times & \times & \times \\ \times & 0 & 0 \\ \times & 0 & \times \end{pmatrix}, D_2 : \begin{pmatrix} \times & \times & \times \\ \times & \times & 0 \\ \times & 0 & 0 \end{pmatrix}; \tag{7}$$

$$E_1 : \begin{pmatrix} 0 & \times & \times \\ \times & 0 & \times \\ \times & \times & \times \end{pmatrix}, E_2 : \begin{pmatrix} 0 & \times & \times \\ \times & \times & \times \\ \times & \times & 0 \end{pmatrix}, E_3 : \begin{pmatrix} 0 & \times & \times \\ \times & \times & 0 \\ \times & 0 & \times \end{pmatrix}; \tag{8}$$

$$F_1 : \begin{pmatrix} \times & 0 & 0 \\ 0 & \times & \times \\ 0 & \times & \times \end{pmatrix}, F_2 : \begin{pmatrix} \times & 0 & \times \\ 0 & \times & 0 \\ \times & 0 & \times \end{pmatrix}, F_3 : \begin{pmatrix} \times & \times & 0 \\ \times & \times & 0 \\ 0 & 0 & \times \end{pmatrix}, \tag{9}$$

Where the crosses “ \times ” imply non-zero arbitrary elements of M_ν . The latest neutrino oscillation data on mixing angles, mass squared differences and cosmology data on sum of absolute neutrino masses allow only six different two-zero textures $A_{1,2}$ and $B_{1,2,3,4}$ as shown by [65, 67].

III. DUNE AT A GLANCE

The Deep Underground Neutrino Experiment (DUNE) is a future accelerator based experiment capable of answering all the three major issues in the neutrino sector mentioned earlier: a) determination of neutrino mass hierarchy, b) resolution of the octant of θ_{23} and c) determination of leptonic CP violation. The first test with the megawatt neutrino-beam facility will begin in ~ 2026 and the experiment itself will be fully operational in ~ 2027 [80, 81]. The DUNE is designed in such a way that it can answer all the three most important questions in the neutrino sector mentioned above. The $\nu_\mu(\bar{\nu}_\mu)$ super-beam from the Fermilab will be detected by a 35-40 kton Liquid Argon (LAr) far detector at a distance of 1300 km in the Homestake mine, South Dakota. The experiment plans to run for 10 years both in anti-neutrino (5 years) and neutrino (5 years) modes. A 1.2 MW - 120 GeV proton beam will deliver 10^{21} protons-on-target (POT) per year which corresponds to a total exposure of 35×10^{22} kton-POT-yr.

All other details, such as signal and background channels, signal efficiencies are taken from [22, 23] and tabulated in table II and table III.

Experiment	Signal	Signal	Background	Calibration error	
		norm error	norm error	Signal	Background
DUNE	ν_e	2%	10%	5%	5%
	ν_μ	5%	10%	5%	5%

TABLE II. Systematics uncertainties for DUNE

Experiment	Signal	Signal	Energy	Runtime (yrs)	Detector Mass (Type)
		Efficiencies	Resolutions	$\nu + \bar{\nu}$	
DUNE	ν_e^{CC}	80%	$0.15/\sqrt{E}$	5 + 5	35 kton (LArTPC)
	ν_μ^{CC}	85%	$0.20/\sqrt{E}$		

TABLE III. Simulation details like signal efficiencies, energy resolutions, total exposures and detector mass for DUNE

IV. NUMERICAL ANALYSIS

In the diagonal charged lepton basis, U_{PMNS} is same as the diagonalising matrix U_ν which can be parametrised as

$$U_{\text{PMNS}} = \begin{pmatrix} c_{12}c_{13} & s_{12}c_{13} & s_{13}e^{-i\delta_{\text{CP}}} \\ -s_{12}c_{23} - c_{12}s_{23}s_{13}e^{i\delta_{\text{CP}}} & c_{12}c_{23} - s_{12}s_{23}s_{13}e^{i\delta_{\text{CP}}} & s_{23}c_{13} \\ s_{12}s_{23} - c_{12}c_{23}s_{13}e^{i\delta_{\text{CP}}} & -c_{12}s_{23} - s_{12}c_{23}s_{13}e^{i\delta_{\text{CP}}} & c_{23}c_{13} \end{pmatrix} \text{diag}(1, e^{i\alpha}, e^{i(\beta+\delta_{\text{CP}})}) \quad (10)$$

where $c_{ij} = \cos \theta_{ij}$, $s_{ij} = \sin \theta_{ij}$. δ_{CP} is the Dirac CP phase and α, β are the Majorana CP phases. Using the parametric form of PMNS matrix shown in (10), the Majorana neutrino mass matrix M_ν can be found as

$$M_\nu = U_{\text{PMNS}} M_\nu^{\text{diag}} U_{\text{PMNS}}^T \quad (11)$$

where

$$M_\nu^{\text{diag}} = \begin{pmatrix} m_1 & 0 & 0 \\ 0 & m_2 & 0 \\ 0 & 0 & m_3 \end{pmatrix}, \quad (12)$$

with m_1, m_2 and m_3 being the three neutrino mass eigenvalues. For the case of normal hierarchy, the three neutrino mass eigenvalues can be written as

$$M_\nu^{\text{diag}} = \text{diag}(m_1, \sqrt{m_1^2 + \Delta m_{21}^2}, \sqrt{m_1^2 + \Delta m_{31}^2})$$

while for the case of inverted hierarchy, they can be written as

$$M_\nu^{\text{diag}} = \text{diag}(\sqrt{m_3^2 + \Delta m_{23}^2 - \Delta m_{21}^2}, \sqrt{m_3^2 + \Delta m_{23}^2}, m_3)$$

The analytical expressions of the elements of this mass matrix are given in Appendix A.

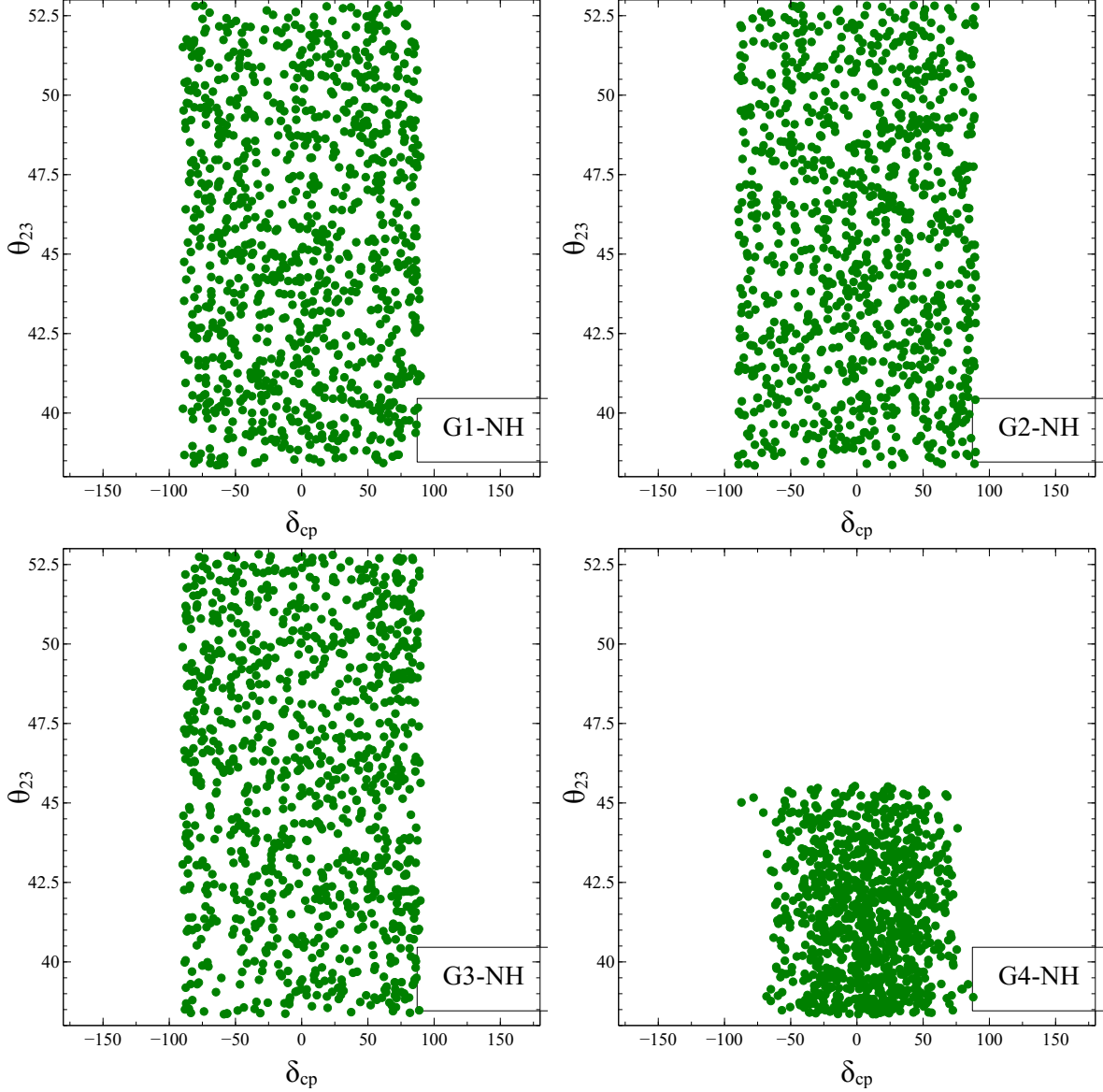


FIG. 1. Neutrino parameters corresponding to one-zero textures for NH

From the parametrisation of light neutrino mass matrix, it can be seen that there are nine parameters: three masses, three angles and three phases. Out of these five parameters namely, two mass squared differences and three mixing angles are measured in several experiments and their best fit values along with 3σ ranges are shown in table I. It is worth noting that there still remains some ambiguity in determining the octant of θ_{23} . Apart from this, the three CP phases and the lightest neutrino mass and hence the type of mass hierarchy

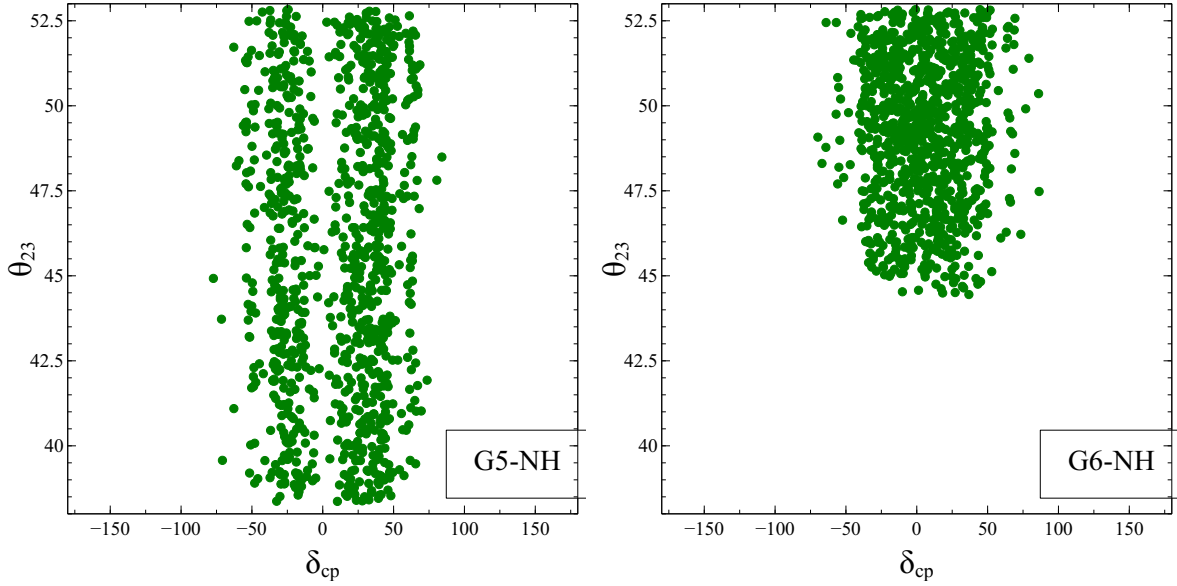


FIG. 2. Neutrino parameters corresponding to one-zero textures for NH

are yet to be determined experimentally. Due to the predictive nature of texture zero mass matrices and upcoming neutrino experiment like DUNE having the potential to settle the issue of θ_{23} octant, Dirac CP phase δ_{cp} as well as mass hierarchy we first numerically evaluate the neutrino parameters for a particular texture zero mass matrix using the 3σ values of two angles θ_{12}, θ_{13} , two mass squared differences from the global fit reference [8]. For each possible one-zero texture mass matrix, we have one complex or two real equations which can be solved numerically to evaluate θ_{23}, δ_{cp} along with restricting other parameters. For the one-zero texture mass matrices, we solve the two real equations corresponding to the texture zero condition and determine the parameter space in terms neutrino parameters. While solving these equations, we vary the lightest neutrino mass in the range $10^{-6} - 0.1$ eV and the Majorana CP phases in the range $-\pi < \alpha, \beta < \pi$.

To use the bound on neutrino parameters from $0\nu\beta\beta$ experiments, we use the standard light neutrino contribution to this rare decay process. This rare decay is a lepton number violating process where a heavier nucleus decays into a lighter one and two electrons $(A, Z) \rightarrow (A, Z + 2) + 2e^-$ without any (anti) neutrinos in the final state thereby violating lepton number by two units. For a review on $0\nu\beta\beta$, please refer to [82]. The amplitude of the light

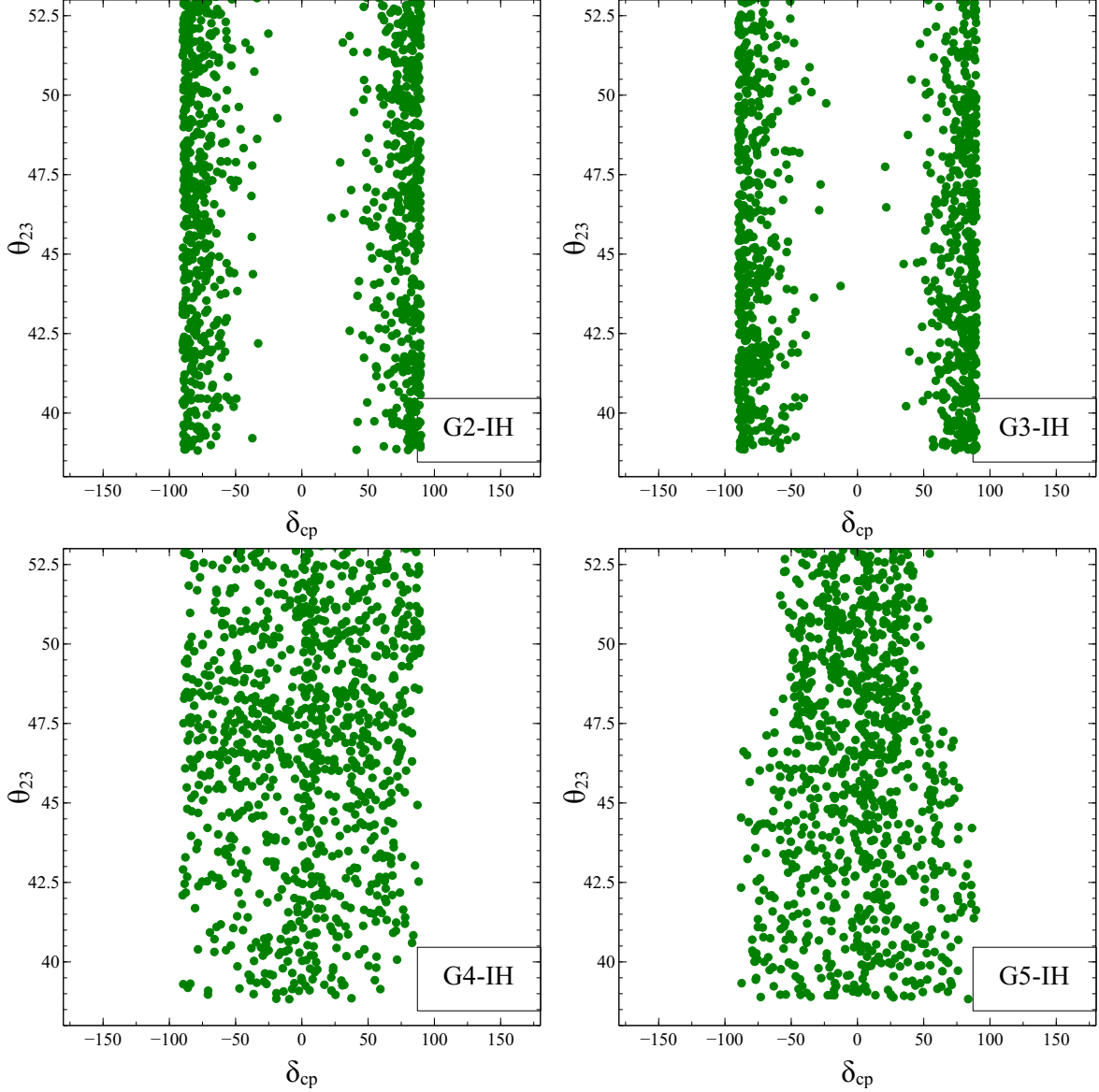


FIG. 3. Neutrino parameters corresponding to one-zero textures for IH

neutrino contribution to $0\nu\beta\beta$ can be written as

$$A_{\nu LL} \propto G_F^2 \sum_i \frac{m_i U_{ei}^2}{p^2} \quad (13)$$

with p being the average momentum exchange for the process. In the above expression, m_i are the masses of light neutrinos for $i = 1, 2, 3$. $G_F = 1.17 \times 10^{-5} \text{ GeV}^{-2}$ is the Fermi coupling constant and $U = U_{\text{PMNS}}$ is the light neutrino mixing matrix. The corresponding

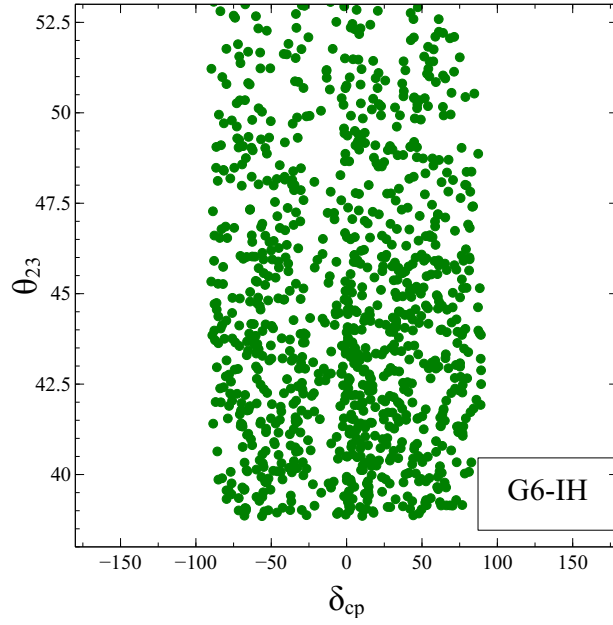


FIG. 4. Neutrino parameters corresponding to one-zero texture G_6 for IH.

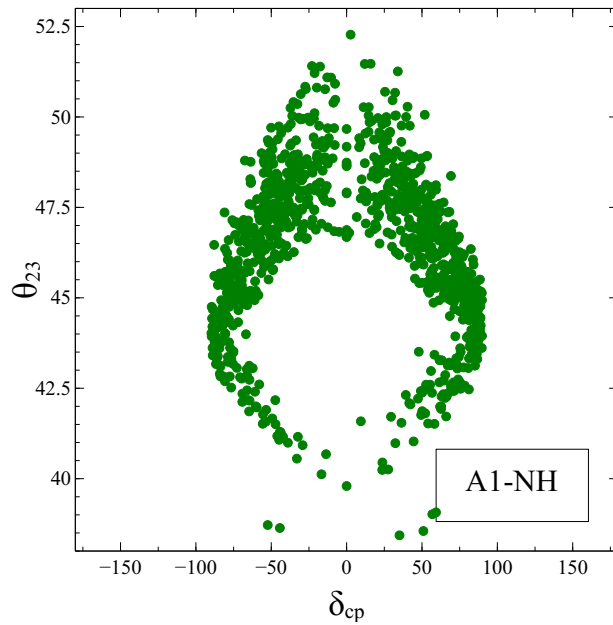


FIG. 5. Neutrino parameters corresponding to two-zero texture A_1 for NH.

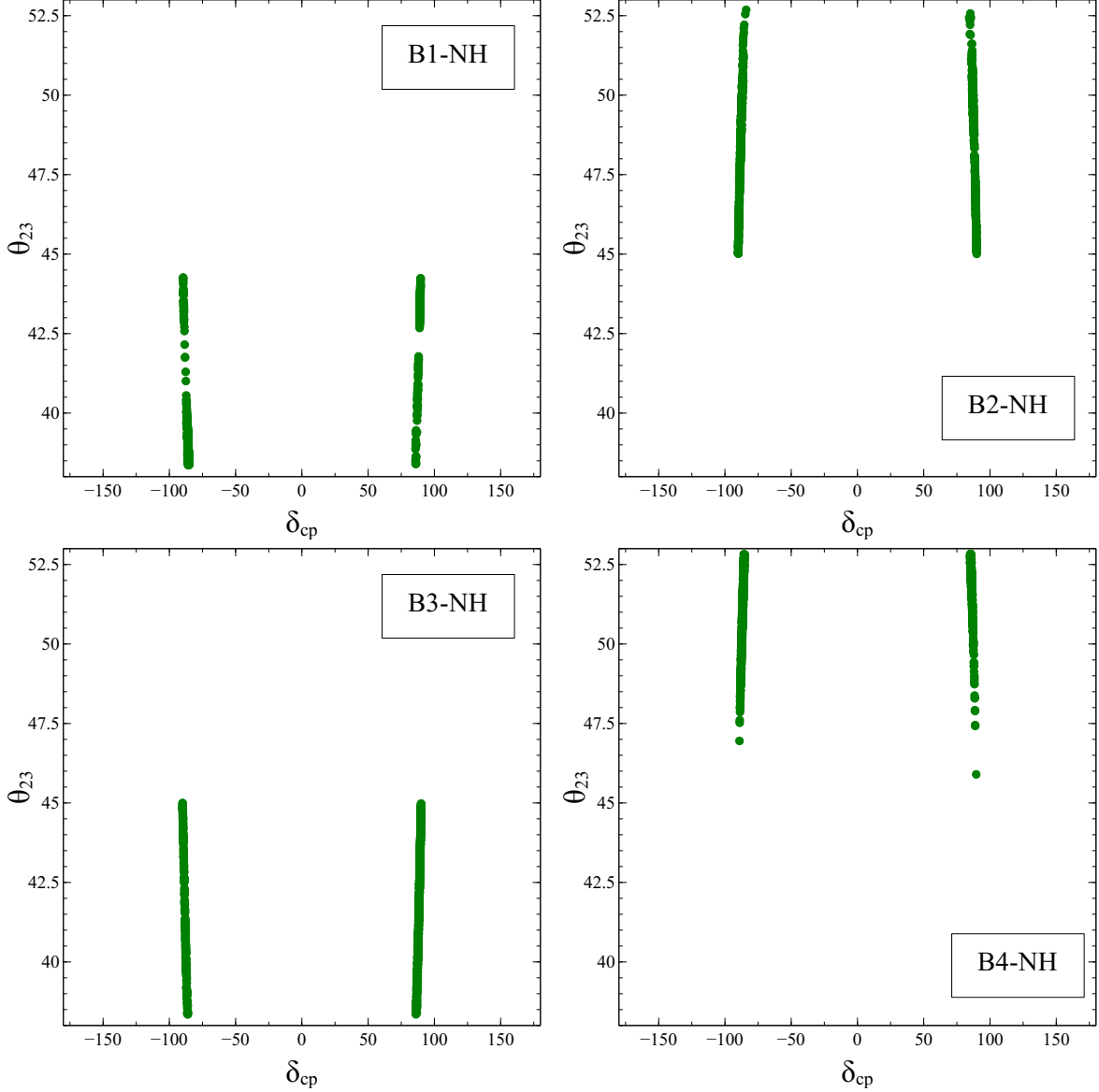


FIG. 6. Neutrino parameters corresponding to two-zero textures for NH

half-life can be written as

$$\frac{1}{T_{1/2}^{0\nu}} = G_{01}^{0\nu} |\mathcal{M}_{\nu}^{0\nu}(\eta_{\nu}^L)|^2 \quad (14)$$

where $\eta_{\nu}^L = \sum_i \frac{m_i U_{ei}^2}{m_e} = \frac{M_{ee}}{m_e}$. Here m_e is the mass of electron, $\mathcal{M}_{\nu}^{0\nu}$ is the nuclear matrix element (NME) and $G_{01}^{0\nu}$ is the phase space factor. Since the ongoing experiments have not observed this rare decay process, they give a lower bound on its half-life or equivalently an

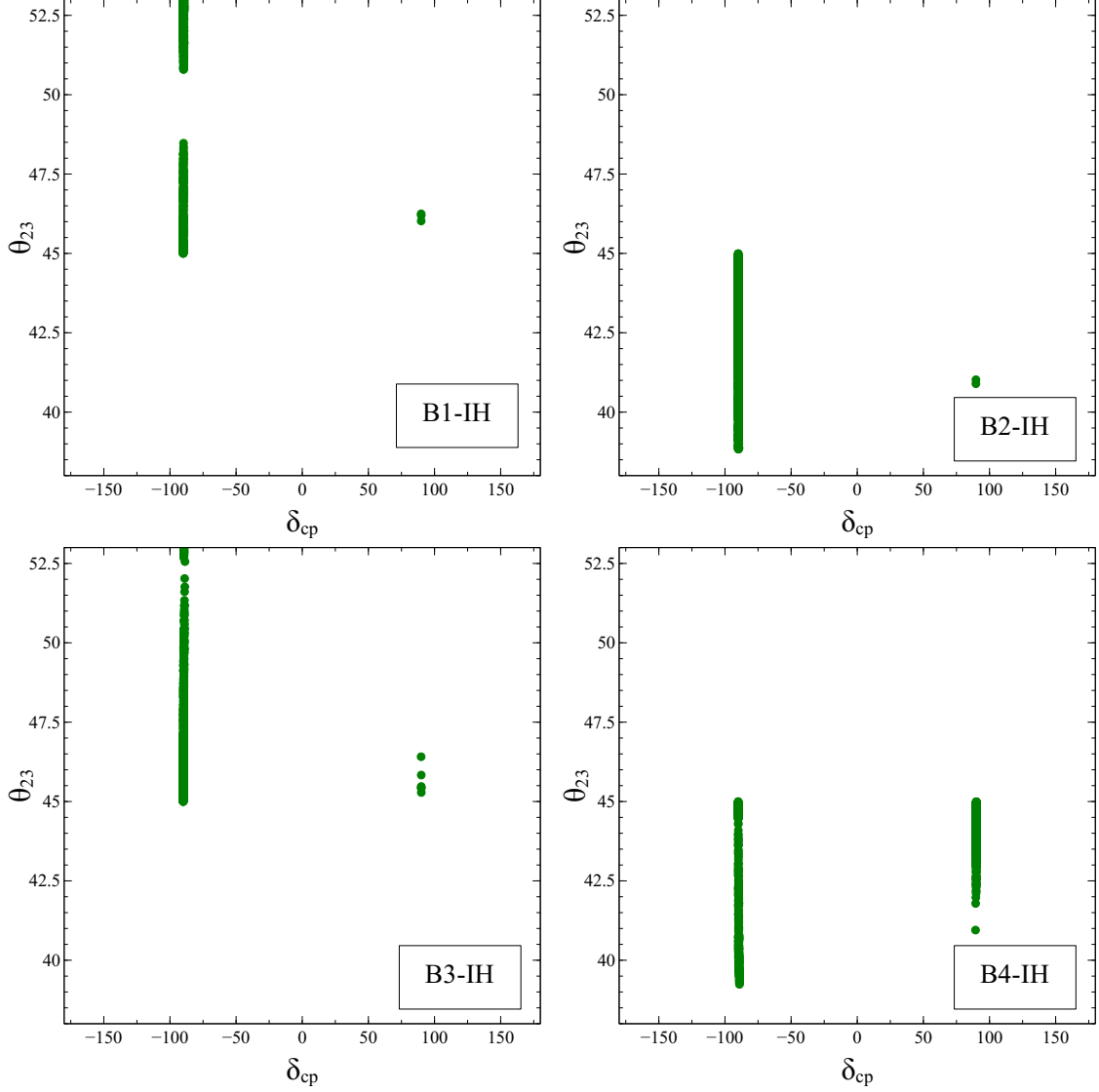


FIG. 7. Neutrino parameters corresponding to two-zero textures for IH

upper bound on the amplitude. The latest data from the KamLAND-Zen experiment in 2016 have given a lower limit on $0\nu\beta\beta$ half-life of $T_{1/2}^{0\nu} > 1.07 \times 10^{26}$ yr at 90% confidence level [12]. Using the commonly adopted values of NME, this lower bound on half-life corresponds to an upper bound on the effective Majorana neutrino mass in the range $|M_{ee}| < 0.061 - 0.165$ eV. More recently in 2017, the GERDA collaboration has given a similar but slightly weaker lower bound on half-life as $T_{1/2}^{0\nu} > 5.3 \times 10^{25}$ yr at 90% confidence level [13] which corresponds to an upper bound $|M_{ee}| < 0.15 - 0.33$ eV. We use the most conservative bound from the

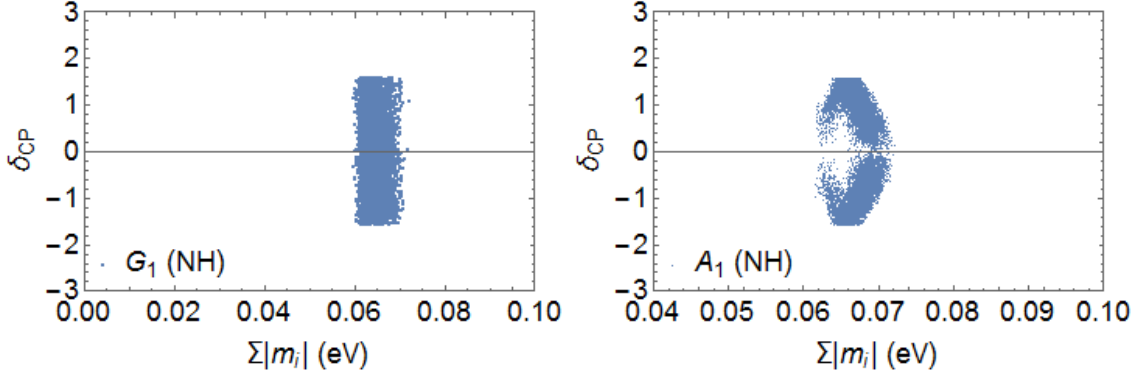


FIG. 8. δ_{CP} with respect to the sum of absolute neutrino masses for the allowed one and two zero textures G_1, A_1 for which $M_{ee} = 0$.

KamLAND-Zen collaboration to constrain the texture zero mass matrices in our analysis. Along with this, we also use the cosmology bound on the sum of absolute neutrino masses $\sum_i |m_i| < 0.17$ eV from the Planck collaboration results [9] that appeared in 2015.

After numerically evaluating the neutrino oscillation parameters for the texture zero mass matrices, we move on to studying the capabilities of DUNE to exclude these textures once it starts taking data. For this, we have used the present best fit values of the standard 3ν oscillation parameters as the ‘true values’ or ‘data’. The best fit values of the oscillation parameters are taken from [8]. To test a particular texture, the values of the neutrino oscillation parameters from the texture zero conditions are used as ‘fit’ values and then χ^2 is calculated between ‘data’ and ‘fit’. We define χ^2 (statistical) as:

$$\chi^2 = \sum_i \sum_{j=1}^2 \frac{[N_{i,j}^{\text{true}} - N_{i,j}^{\text{test}}]^2}{N_{i,j}^{\text{true}}}, \quad (15)$$

where $N_{i,j}^{\text{true}}$ and $N_{i,j}^{\text{test}}$ are the event rates that correspond to ‘data’ and ‘fit’. Here, index i corresponds to the number of bins and j corresponds to the type of neutrinos i.e. $j = 1$ for neutrinos and $j = 2$ for antineutrinos. We have considered 39 bins for DUNE in the energy range 0.5 – 10 GeV having bin width of 250 MeV. The systematics uncertainties like signal and background related uncertainties, calibration errors are introduced in the χ^2 by pull method and they are allowed to deviate from their standard values in the calculation of the expected rate in the $\{i, j\}$ -th bins $N_{i,j}^{\text{test}}$. If the k^{th} input gets deviated from its standard

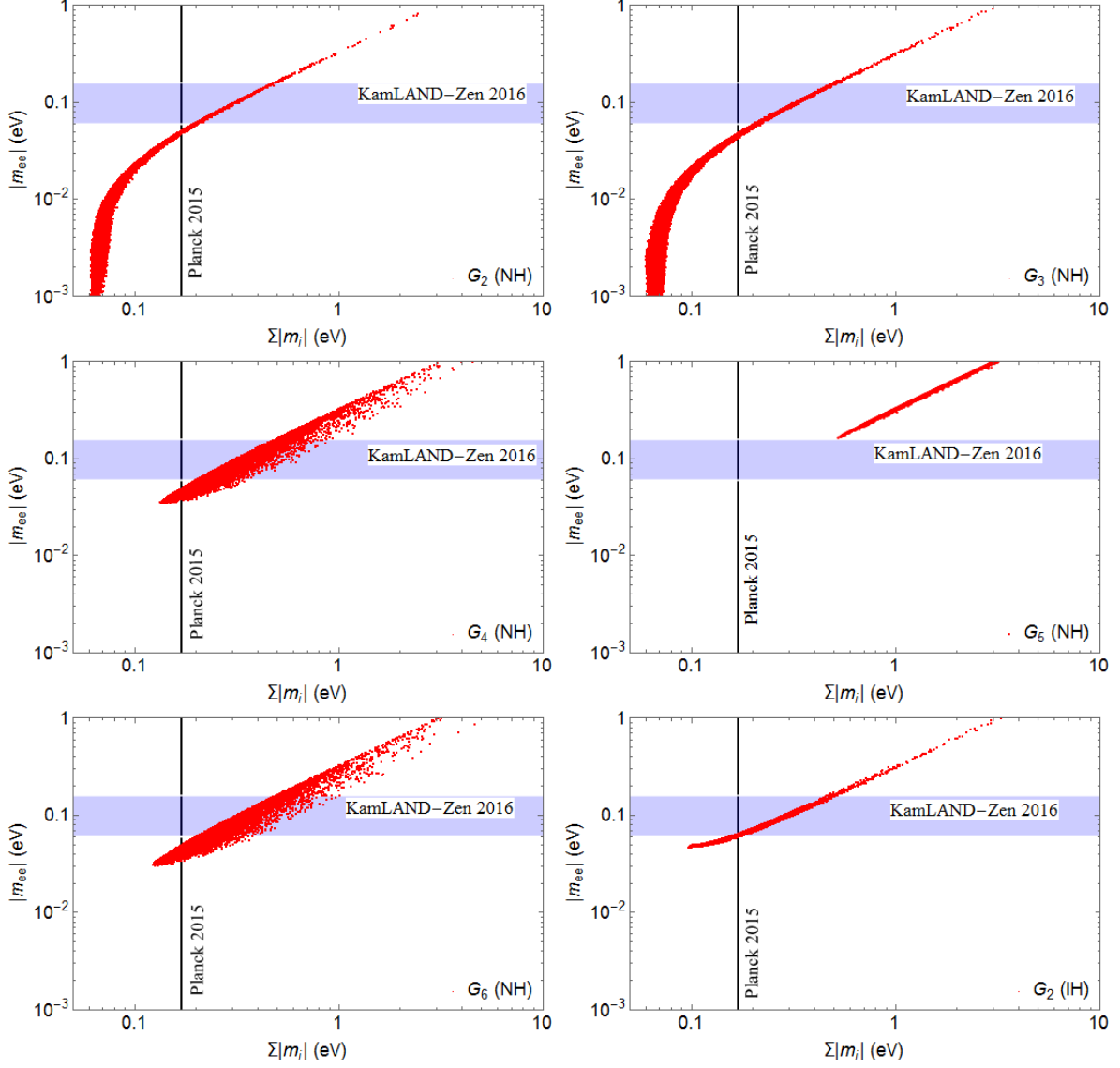


FIG. 9. The contribution to $0\nu\beta\beta$ for one zero texture mass matrices shown with respect to the sum of absolute neutrino masses. The blue horizontal band corresponds to the 2016 KamLAND-Zen bound $|M_{ee}| < 0.061 - 0.165$ eV. The vertical solid black line corresponds to the Planck 2015 bound $\sum_i |m_i| < 0.17$ eV.

value by $\sigma_k \xi_k$, then our final modified χ^2 will be:

$$\chi^2(\xi_k) = \sum_i \sum_{j=1}^2 \frac{[N_{i,j}^{test}(std) + \sum_{k=1}^{npull} C_{i,j}^k \xi_k - N_{i,j}^{true}]}{N_{i,j}^{true}} + \sum_{k=1}^{npull} \xi_k^2$$

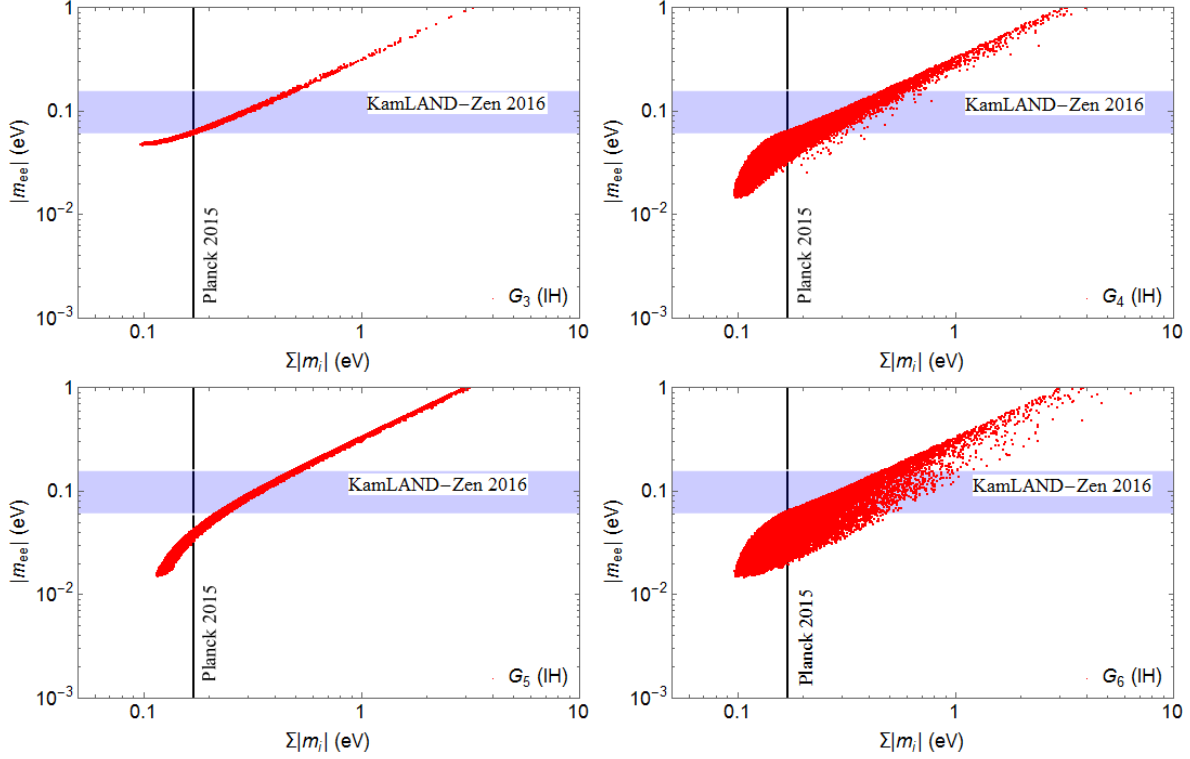


FIG. 10. The contribution to $0\nu\beta\beta$ for one zero texture mass matrices shown with respect to the sum of absolute neutrino masses. The blue horizontal band corresponds to the 2016 KamLAND-Zen bound $|M_{ee}| < 0.061 - 0.165$ eV. The vertical solid black line corresponds to the Planck 2015 bound $\sum_i |m_i| < 0.17$ eV.

and hence,

$$\chi_{\text{pull}}^2 = \min_{\xi_k} [\chi^2(\xi_k)]$$

Here, $N_{i,j}^{test}(std)$ is the events corresponding to ‘fit’ in $\{i, j\}$ -th bin computed with the standard values of the inputs, npull is the no of uncertainties, σ_k is the uncertainties associated with the k^{th} inputs. ξ_k are the pull variables or nuisance parameters and they are measure of how k^{th} inputs deviates from its standard value. They describe how the event rates depends on the various sources of systematical errors. In the expression, $c_{i,j}^k$ is the change in the expected event spectra when the k^{th} input changes by σ_k . Nuisance systematic parameters are given in table II. Since, we are testing each textures at DUNE and hence all the ‘fit values’ of the oscillation parameters are as predicted by the texture zero conditions. We

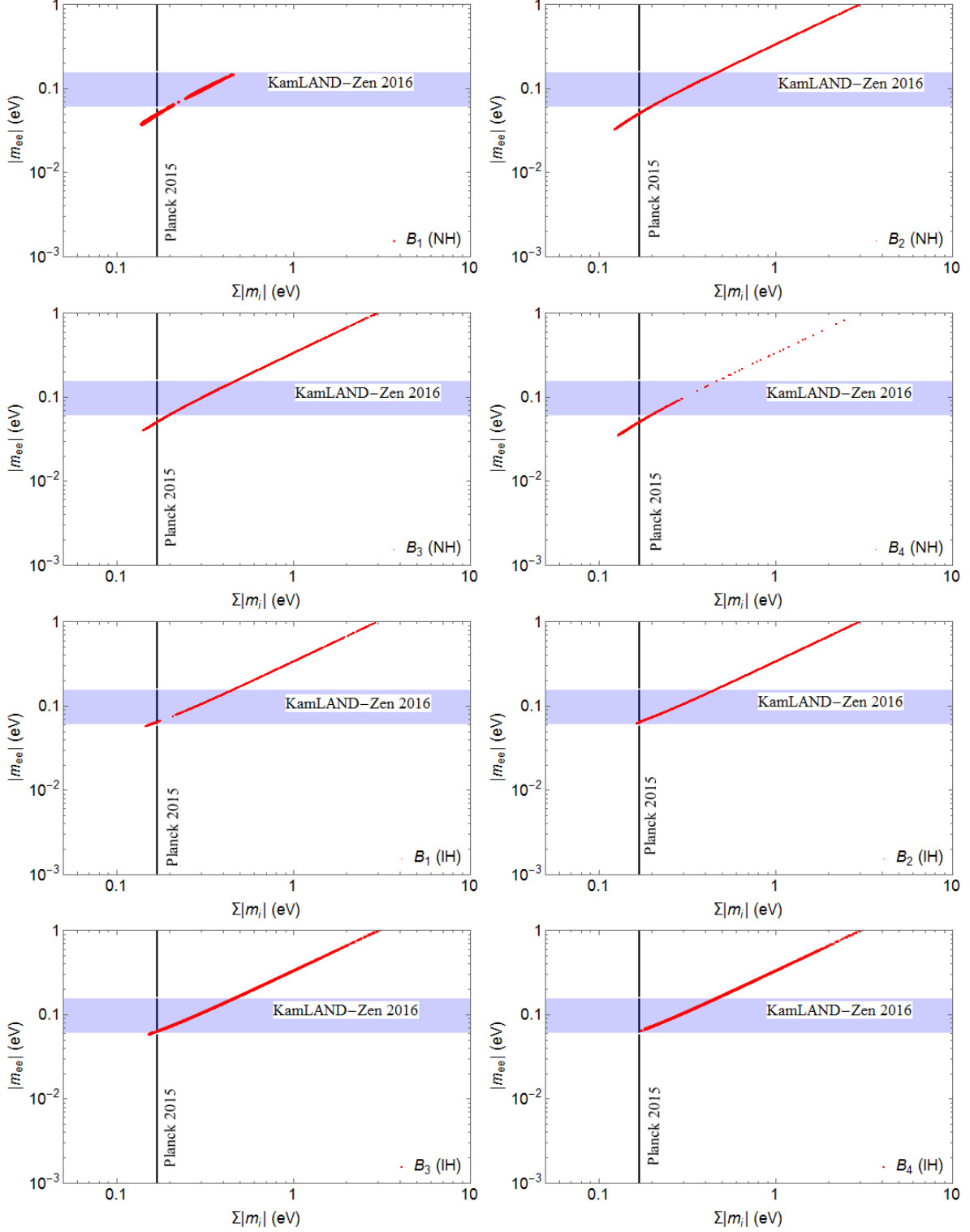


FIG. 11. The contribution to $0\nu\beta\beta$ for two zero texture mass matrices shown with respect to the sum of absolute neutrino masses. The blue horizontal band corresponds to the 2016 KamLAND-Zen bound $|M_{ee}| < 0.061 - 0.165$ eV. The vertical solid black line corresponds to the Planck 2015 bound $\sum_i |m_i| < 0.17$ eV.

have not considered any priors on them in this analysis. Variation of all the six neutrino oscillation parameters are taken into account in ‘fit’ according to texture zero conditions.

V. RESULTS AND DISCUSSIONS

A. Allowed Texture Zero Mass Matrices

In this subsection, we discuss the results we obtain for the first part of our analysis that is, constraining the texture zero mass matrices from the latest experimental bounds on neutrino oscillation parameters, sum of absolute neutrino masses and $0\nu\beta\beta$ half-life.

For one zero texture mass matrices, we numerically solve the two real texture zero equations or one complex texture zero condition. We solve it for two parameters while randomly varying other parameters in their allowed 3σ range. The lightest neutrino mass is varied in the range $10^{-6} - 0.1$ eV. For the texture zero mass matrices allowed by neutrino oscillation data alone, we show the corresponding regions of parameter space in $\theta_{23} - \delta_{cp}$ plane in figure 1, 2, 3, 4 for both NH and IH. It should be noted that due to only two real constraint equations and more unknown neutrino parameters, the one-zero textures are not very predictive. This is obvious from the broad ranges of values allowed in the $(\theta_{23}, \delta_{cp})$ plane. We find that the latest neutrino oscillation data allow all the one zero texture mass matrices except G_1 with IH.

Similarly, we numerically solve the two complex or four real equations for the two-zero texture mass matrices $A_{1,2}, B_{1,2,3,4}$ and extract the resulting parameter space. In this case also, we vary the lightest neutrino mass in the range $10^{-6} - 0.1$ eV and solve the four real equations numerically in order to evaluate θ_{23}, δ_{cp} along with two Majorana phases. They are shown in figure 5, 6, 7 for both NH and IH. Since there are four real constraint equations, two zero texture mass matrices are much more predictive as can be seen from the narrow range of parameters allowed from the texture zero conditions. We find that the use of the latest 3σ global fit values of solar and reactor mixing angles as well as the two mass squared differences allow only five two-zero textures with NH and four two-zero textures with IH. This is in contrast with the allowed two-zero texture matrices shown in earlier works [65] as we are using more precise values of neutrino oscillation parameters from the latest global fit data. The allowed textures we have got from fitting neutrino oscillation data are same

as the ones obtained in the more recent work [67]. This relatively recent work [67] however did not include the textures $A_{1,2}$ in their analysis as they correspond to vanishing amplitude for $0\nu\beta\beta$. Here we include them and found the A_1 texture to be allowed in case of normal hierarchy. It should be noted that for all these plots in figure 1, 2, 3, 4, 5, 6, 7 we have not imposed the constraints from the Planck and KamLAND-Zen experiments on sum of absolute neutrino masses and effective light neutrino mass respectively. At this stage the viability of the Majorana texture zero mass matrices is studied only in the light of latest neutrino oscillation data.

After finding the allowed texture zero mass matrices from the requirement of satisfying the latest neutrino oscillation data, we further check their viabilities in the light of cosmology and $0\nu\beta\beta$ bounds mentioned before. Since the textures G_1, A_1 predict vanishing $0\nu\beta\beta$ amplitude, we show δ_{cp} versus sum of absolute neutrino masses for these two textures in figure 8. We find that all the points allowed from neutrino data also obey the Planck 2015 upper bound on $\sum_i |m_i|$. The contributions to $0\nu\beta\beta$ are shown in figure 9, 10, 11. It is interesting to see from figure 9, 10 and 11 that most of the texture zero mass matrices can saturate the experimental bounds on $0\nu\beta\beta$ as well as the sum of absolute neutrino masses. The two zero texture mass matrix A_1 however predicts $\sum_i |m_i|$ far below the Planck 2015 bound. We find that one texture zero mass matrix belonging to previously allowed one zero texture mass matrices become disallowed after incorporating these additional constraints. This is namely, the G_5 texture with normal hierarchy as seen from figure 9. If we consider the most conservative KamLAND-Zen bound corresponding to the lower most value of $|M_{ee}|$ in the blue band shown in figure 9, 10 and 11 then two texture zero mass matrices belonging to previously allowed two zero texture mass matrices become disallowed. They are namely, B_2 and B_4 with inverted hierarchy as seen from figure 11. In fact B_4 texture with inverted hierarchy is disallowed from the Planck 2015 bound as seen from the same figure 11. Thus, all the two zero texture mass matrices with NH studied in this work are allowed except A_2 and three such texture zero matrices with IH namely $B_{1,2,3}$ are allowed. In our subsequent analysis from the DUNE point of view, we will consider these allowed texture zero mass matrices only.

We finally summarise our results from first part of our analysis in the table IV and table V for one zero and two zero texture mass matrices respectively.

Patterns	Neutrino Data IH (NH)	$0\nu\beta\beta$ Bound IH (NH)	Planck Bound IH (NH)
G_1	$\times(\checkmark)$	$\times(\checkmark)$	$\times(\checkmark)$
G_2	$\checkmark(\checkmark)$	$\checkmark(\checkmark)$	$\checkmark(\checkmark)$
G_3	$\checkmark(\checkmark)$	$\checkmark(\checkmark)$	$\checkmark(\checkmark)$
G_4	$\checkmark(\checkmark)$	$\checkmark(\checkmark)$	$\checkmark(\checkmark)$
G_5	$\checkmark(\checkmark)$	$\checkmark(\times)$	$\checkmark(\times)$
G_6	$\checkmark(\checkmark)$	$\checkmark(\checkmark)$	$\checkmark(\checkmark)$

TABLE IV. Summary of results for one zero texture with inverted and normal hierarchy. The symbol \checkmark (\times) is used when the particular texture zero mass matrix is (not) consistent with the respective experimental bound.

Patterns	Neutrino Data IH (NH)	$0\nu\beta\beta$ Bound IH (NH)	Planck Bound IH (NH)
A_1	$\times(\checkmark)$	$\times(\checkmark)$	$\times(\checkmark)$
A_2	$\times(\times)$	$\times(\times)$	$\times(\times)$
B_1	$\checkmark(\checkmark)$	$\checkmark(\checkmark)$	$\checkmark(\checkmark)$
B_2	$\checkmark(\checkmark)$	$\checkmark(\checkmark)$	$\checkmark(\checkmark)$
B_3	$\checkmark(\checkmark)$	$\checkmark(\checkmark)$	$\checkmark(\checkmark)$
B_4	$\checkmark(\checkmark)$	$\checkmark(\checkmark)$	$\times(\checkmark)$

TABLE V. Summary of results for two zero texture with inverted and normal hierarchy. The symbol \checkmark (\times) is used when the particular texture zero mass matrix is (not) consistent with the respective experimental bound. The \checkmark in red colour means that the particular texture is only marginally allowed due to the broad band of upper bound on M_{ee} from $0\nu\beta\beta$ experiment.

B. Probe of Allowed Textures at DUNE

In this section, we present our results. We have tested two possible texture zero mass matrices at DUNE namely, one-zero and two-zero. Each set of textures are tested for both the hierarchies.

In fig. 12, we show the exclusion of G_1 , G_2 , G_3 , G_4 and G_6 textures (generated assuming true NH) while in fig. 13, the allowed/exclusion regions are shown at DUNE in $\theta_{23} - \delta_{cp}$ parameter space. The solid green (blue) line corresponds to true $\theta_{23} = 41.6^\circ$ (48.4°) i.e. θ_{23}

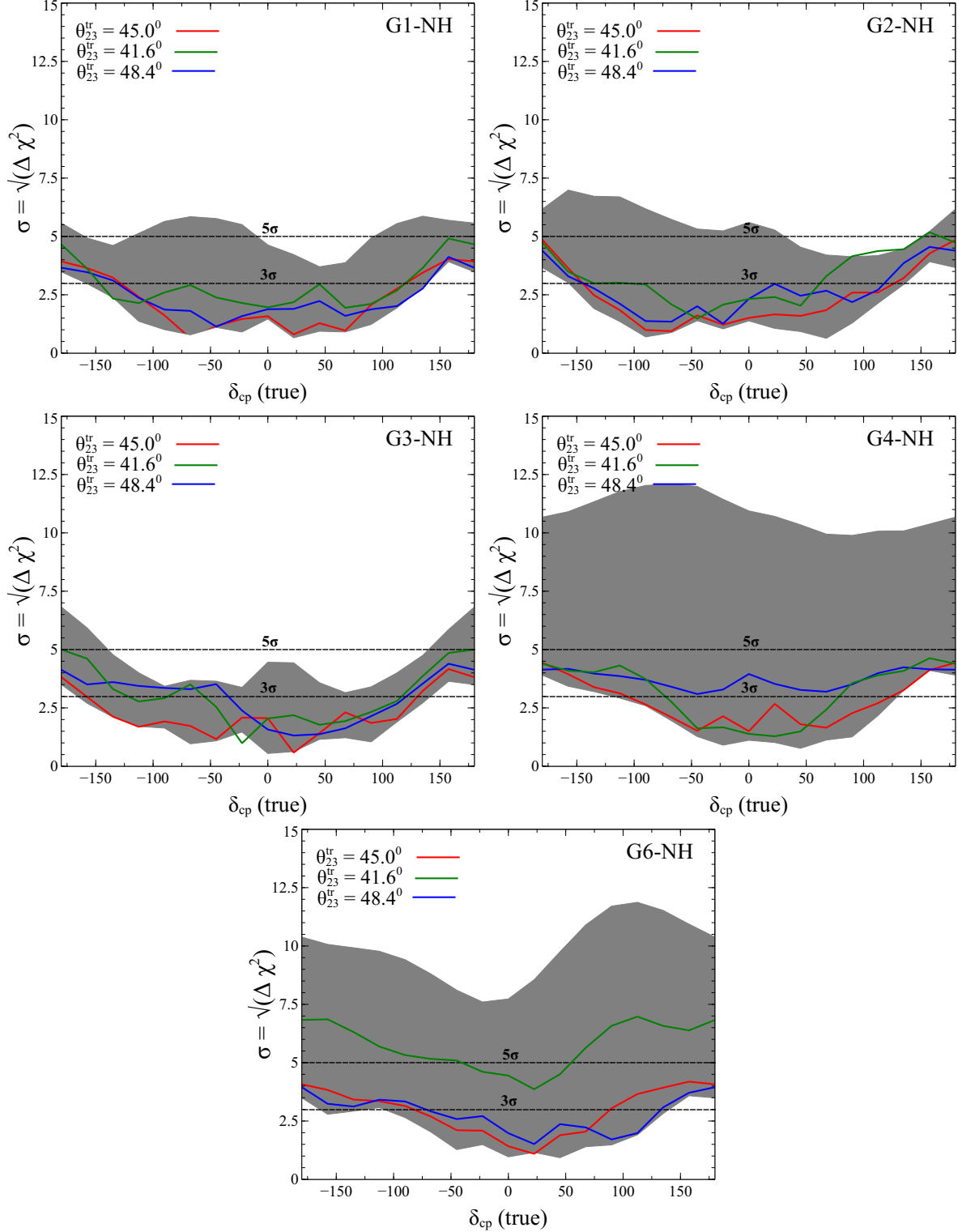


FIG. 12. The exclusion of different one-zero textures at DUNE assuming NH as the true hierarchy. The grey band represents the full variation of θ_{23} in its 3σ allowed range. Green, blue and the red plots corresponds to three different choice of θ_{23} i.e. green plot is for the best fit value of θ_{23} in the LO while the blue plot is for θ_{23} in the HO. The red plot is for maximal θ_{23} .

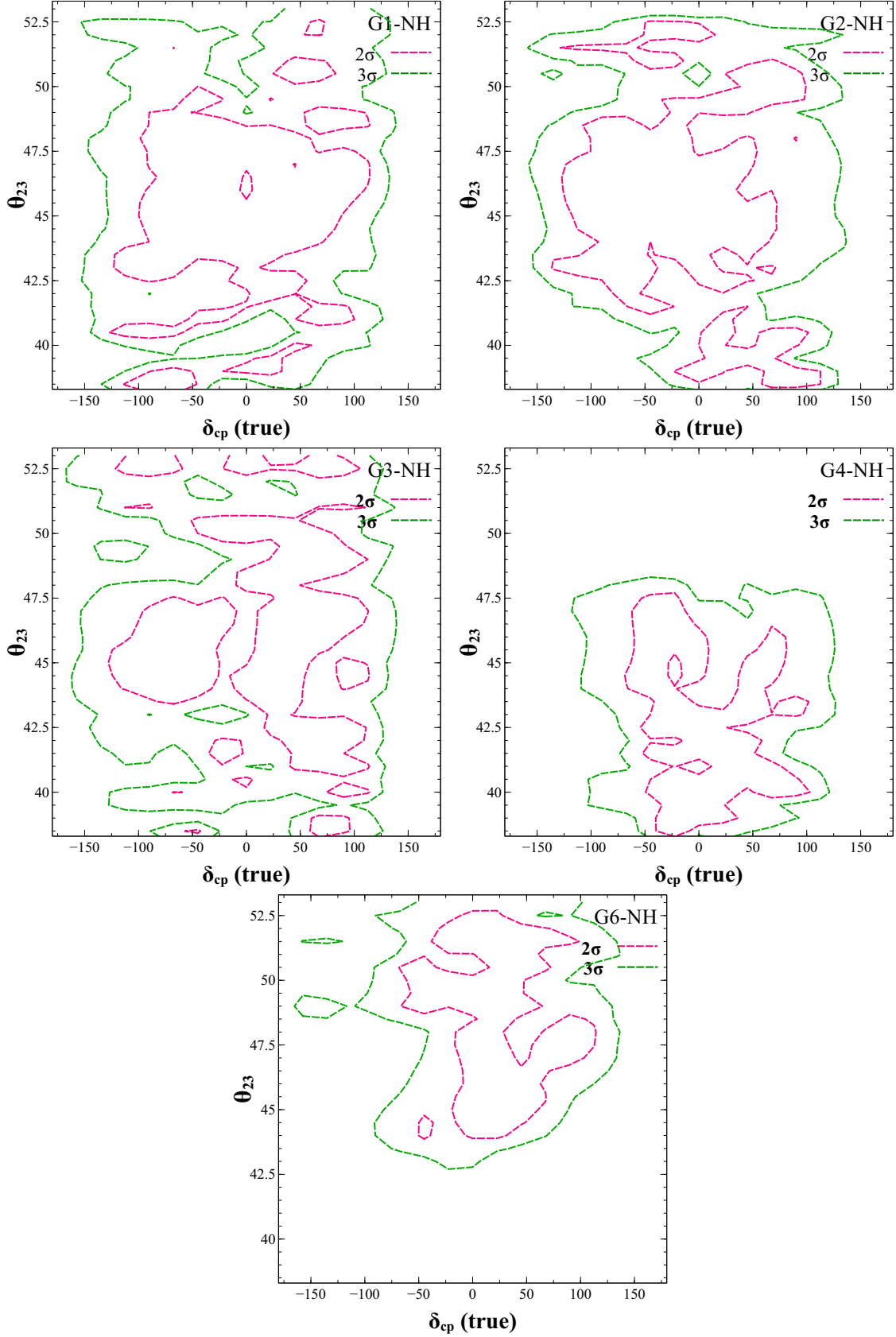


FIG. 13. In the contour plots, we show the allowed regions corresponding to different one-zero textures in NH mode. The green (red) dotted line represents the 3σ (2σ) contour at 1 d.o.f..

in the LO (HO) and the red line corresponds to maximal θ_{23} i.e. $\theta_{23} = 45^\circ$. For each true δ_{cp} , the grey band show the minimum and maximum of χ_{min}^2 corresponding to variation of θ_{23} in its 3σ allowed range. In case of G1, G2 and G3, only a small portion of the grey band lies above 5σ C.L., while for G4 and G6 texture, a large fraction of χ_{min}^2 lies above the 5σ . All the region that lies above the 5σ (3σ) black line is excluded at 5σ (3σ). So for most of the true θ_{23} , DUNE can exclude G4 and G6 at 5σ C.L. for all true δ_{cp} . For the three special cases, we see that except $\theta_{23} = 41.6^\circ$ in G6-NH, DUNE can not exclude these textures at 5σ for almost all true δ_{cp} . But for $\theta_{23} = 41.6^\circ$, DUNE can exclude G6-NH at 5σ for some of the true δ_{cp} except a small fraction around $\delta_{\text{cp}} = 0$. The contours shown in fig. 13 are defined by $\chi^2 > 4$ (9) which corresponds to 2σ (3σ) C.L.. So for a given texture and for a given set of true θ_{23} and δ_{cp} , if the $\chi^2 > 4$ (9), then we can say that the texture can be excluded at 2σ (3σ) C.L.. It is observed from the contour plots in fig. 13 that DUNE can exclude G4 (G6) texture in NH mode approximately for all true δ_{cp} if true $\theta_{23} > 48.5^\circ$ ($\theta_{23} < 43.5^\circ$) at 3σ C.L.. It is difficult to draw such concluding remarks for G1, G2 and G3 as most of the $\theta_{23} - \delta_{\text{cp}}$ parameter space is allowed at $2\sigma/3\sigma$ C.L. as seen from the contour plot in fig. 12.

In fig. 14 and 15, we show our results for G2, G3, G4, G5 and G6 textures assuming true IH. Here also, the green (blue) line represents the best fit value of $\theta_{23} = 40.0^\circ$ (50.0°) in the LO (HO) and the red line corresponds to maximal θ_{23} i.e. $\theta_{23} = 45^\circ$. The predictivity of these textures are less as most of the $\theta_{23} - \delta_{\text{cp}}$ parameter space is allowed at 3σ . But DUNE can exclude G2 and G3 at 3σ for any θ_{23} at the CP conserving values of δ_{cp} while G4, G5 and G6 are excluded for $\delta_{\text{cp}} = \pm\pi$ at 3σ for all θ_{23} .

In fig. 16, we present our results for the two-zero textures: A1, B1, B2, B3 and B4 assuming true NH. The behaviour of the grey band is very much similar in case of B1, B2, B3 and B4 and the most of the $\theta_{23} - \delta_{\text{cp}}$ parameter space is excluded at DUNE at 3σ . For $\theta_{23} = 41.6^\circ$, DUNE can exclude B1, B2 and B4 at 3σ for all true δ_{cp} . Similarly, B1 and B3 is possible to exclude at 3σ for all δ_{cp} if $\theta_{23} = 48.4$. As seen from the contour plots in fig. 17, B1 is more predictive compared to all other two-zero texture in NH mode, as most of the $\theta_{23} - \delta_{\text{cp}}$ parameter space is excluded at 3σ . Almost, for any θ_{23} in HO, DUNE can exclude B1 for all true values of δ_{cp} at 2σ as seen from fig. 17. For any $\theta_{23} > 51.5^\circ$ and $\theta_{23} < 42.5^\circ$, DUNE can exclude B2 for all true δ_{cp} at 3σ C.L.. Similarly, DUNE can exclude both B3 and B4 for all true δ_{cp} at 3σ , if $\theta_{23} > 48.5^\circ$ and $\theta_{23} < 42.5^\circ$ respectively. A1 is less predictive as it allows most of the $\theta_{23} - \delta_{\text{cp}}$ parameter space at 3σ . Except A1, all other

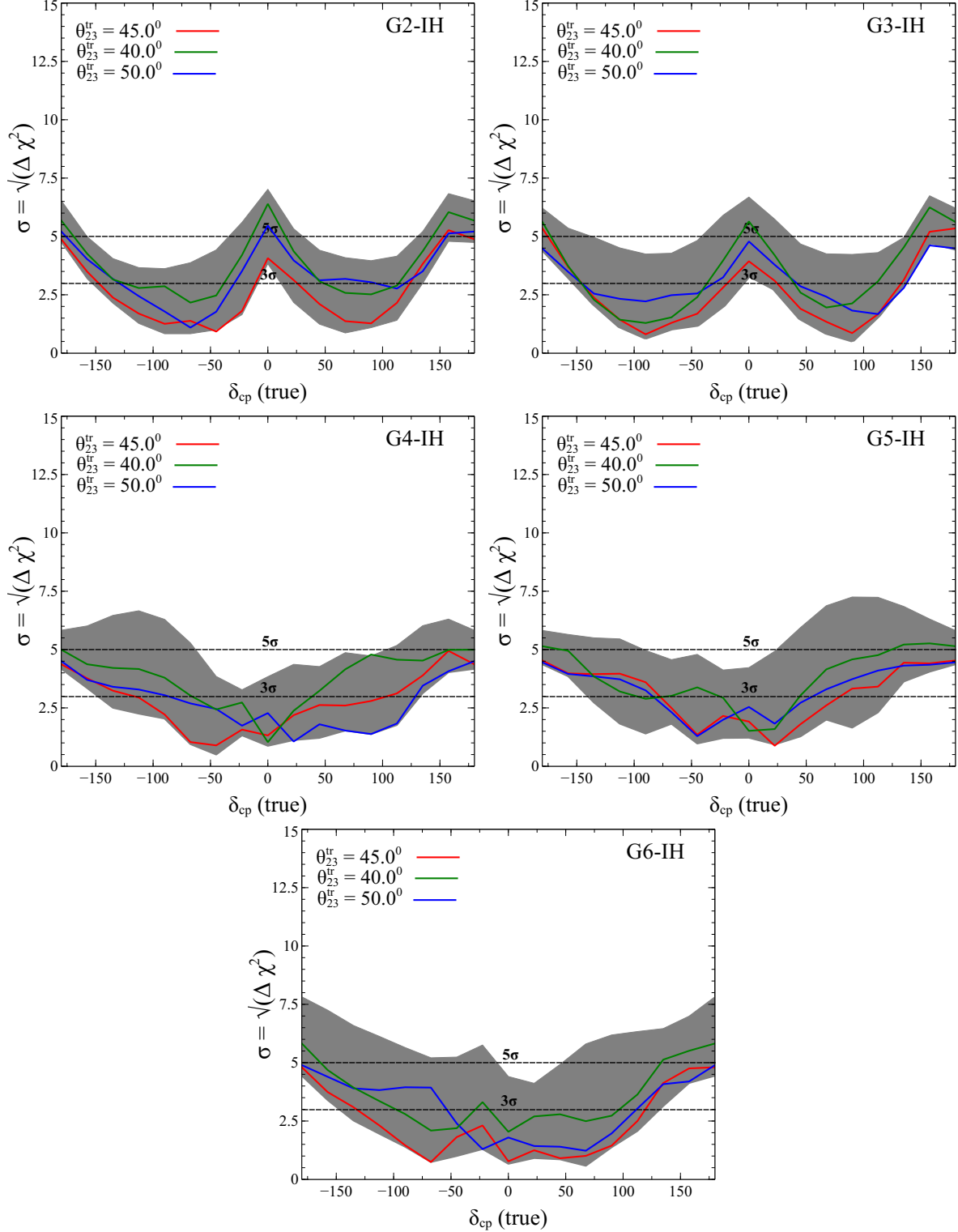


FIG. 14. The exclusion of different one-zero textures at DUNE assuming IH as the true hierarchy. The grey band represents the full variation of θ_{23} in its 3σ allowed range. Green, blue and the red plots corresponds to three different choice of θ_{23} i.e. green plot is for the best fit value of θ_{23} in the LO while the blue plot is for θ_{23} in the HO. The red plot is for maximal θ_{23} .

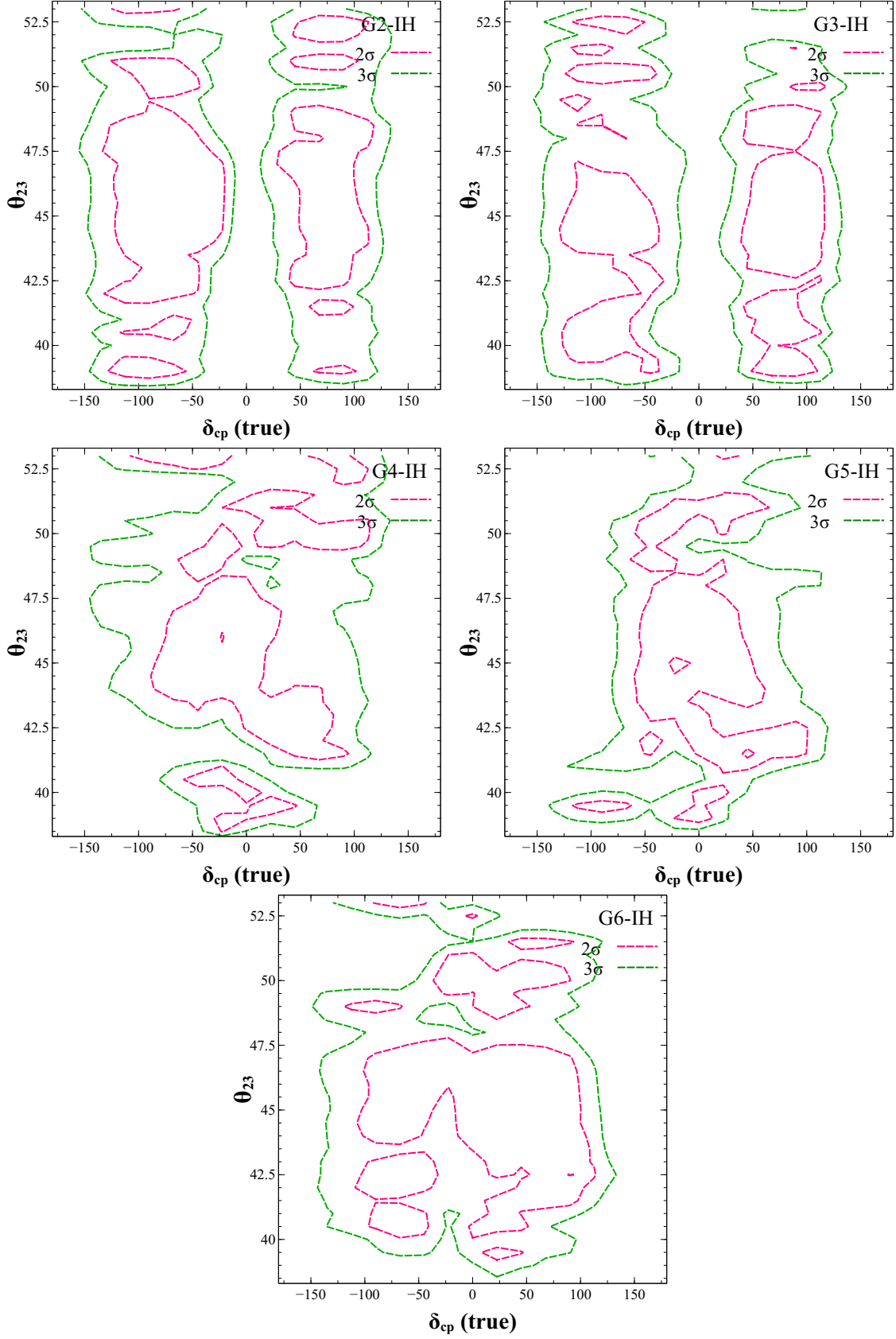


FIG. 15. In the contour plots, we show the allowed regions corresponding to different one-zero textures in IH mode. The green (red) dotted line represents the 3σ (2σ) contour at 1 d.o.f.

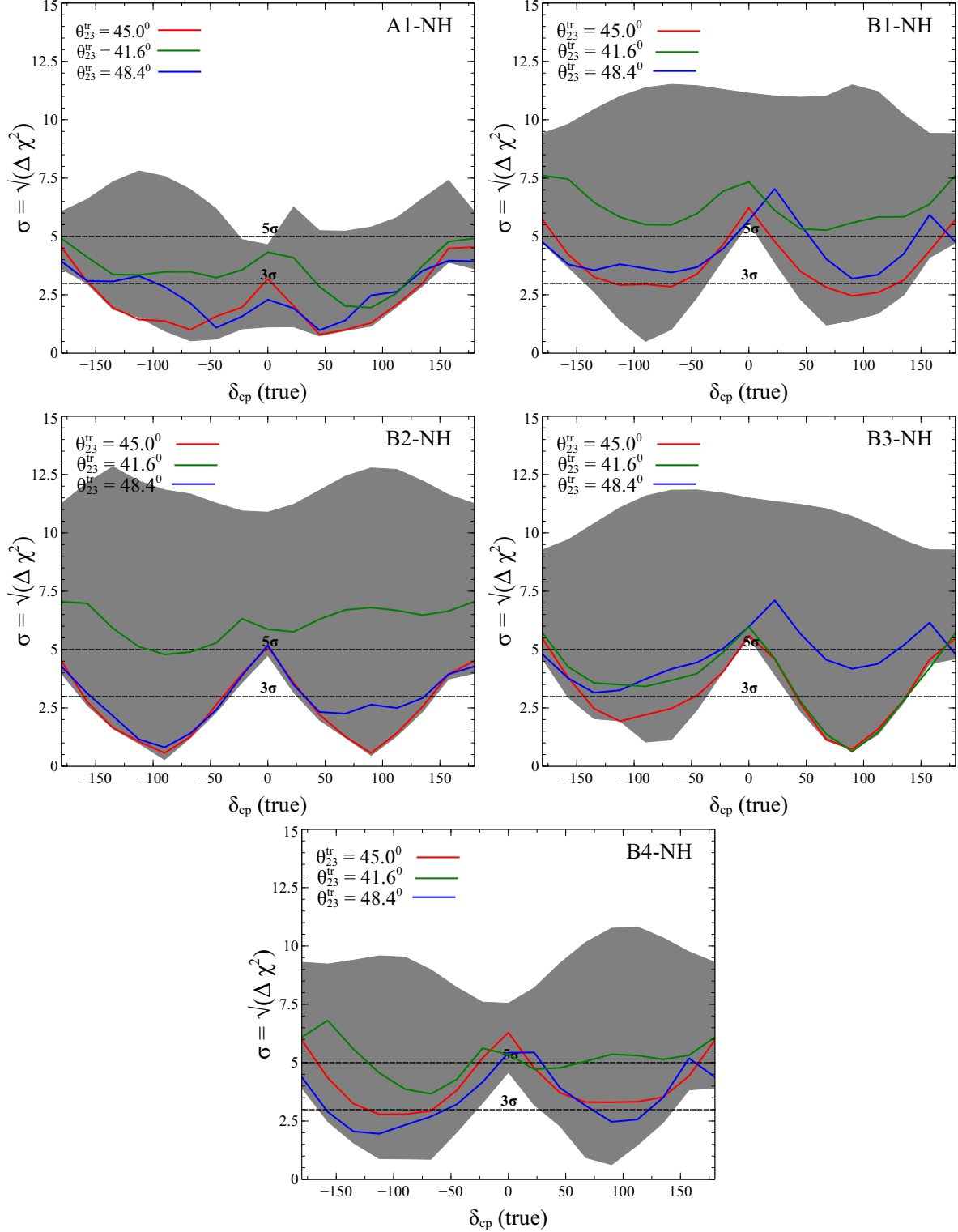


FIG. 16. The exclusion of different two-zero textures at DUNE assuming NH as the true hierarchy. In the upper panel, the grey band represents the full variation of θ_{23} in its 3σ allowed range. Green, blue and the red plots corresponds to three different choice of θ_{23} i.e. green plot is for the best fit value of θ_{23} in the LO while the blue plot is for θ_{23} in the HO. The red plot is for maximal θ_{23} .

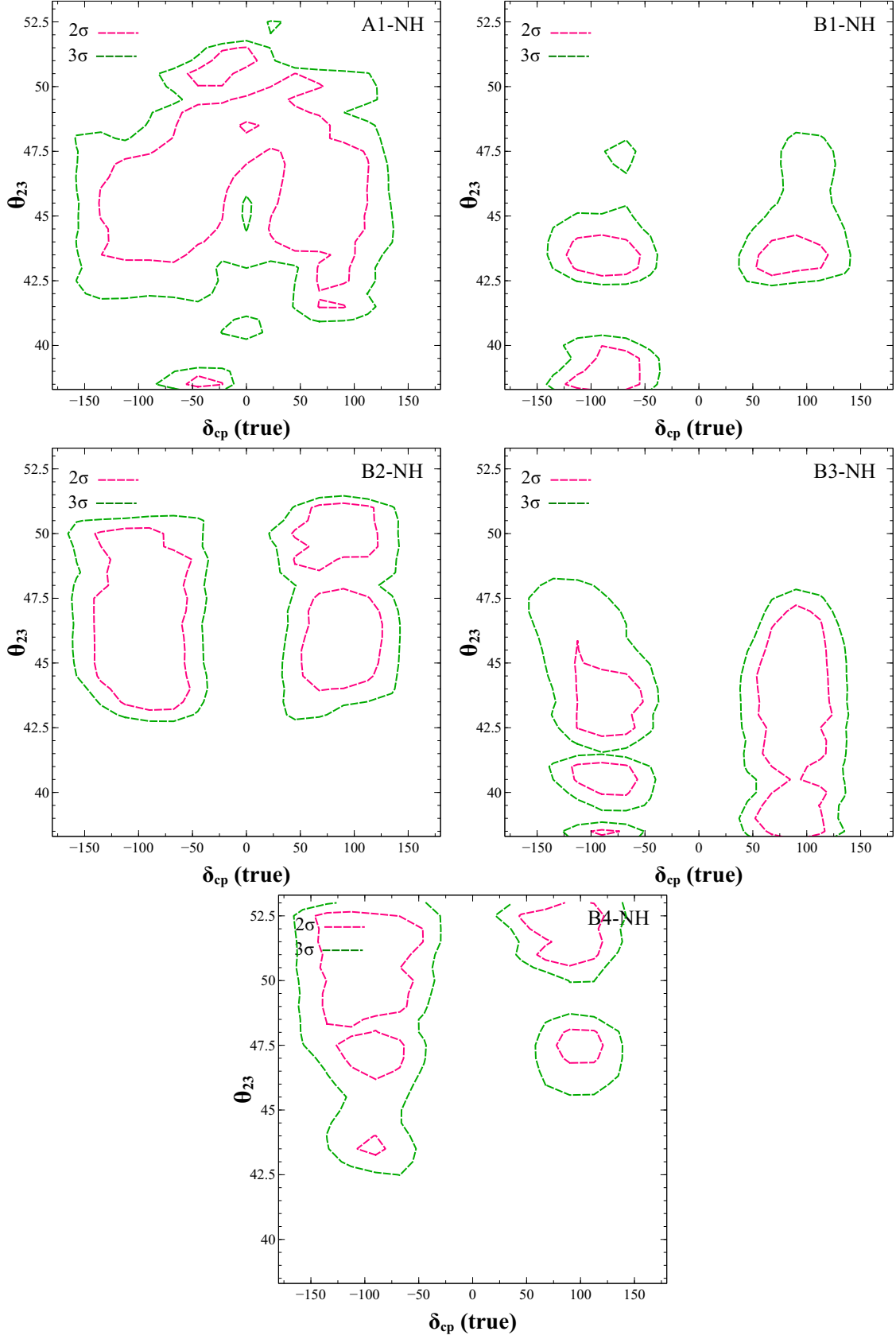


FIG. 17. In the contour plots, we show the allowed regions corresponding to different two-zero textures in NH mode. The green (red) dotted line represents the 3σ (2σ) contour at 1 d.o.f.

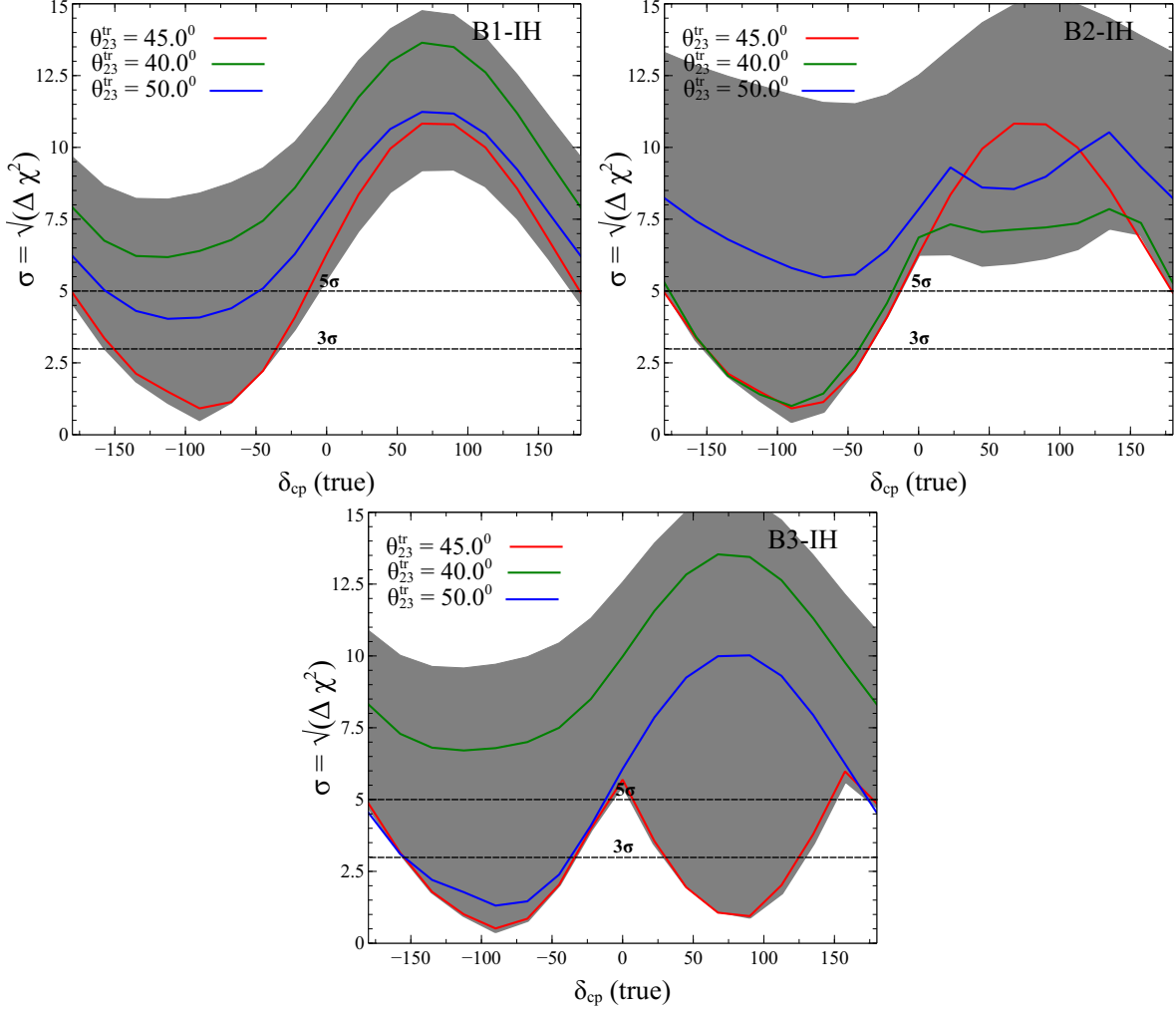


FIG. 18. The exclusion of different two-zero textures at DUNE assuming IH as the true hierarchy. In the upper panel, the grey band represents the full variation of θ_{23} in its 3σ allowed range. Green, blue and the red plots corresponds to three different choice of θ_{23} i.e. green plot is for the best fit value of θ_{23} in the LO while the blue plot is for θ_{23} in the HO. The red plot is for maximal θ_{23} .

two-zero textures in NH mode are excluded at DUNE for the CP conserving values almost at 5σ C.L.(see fig. 16).

In fig. 18 and 19, we have shown our results for B1, B2 and B3 textures assuming IH as the true hierarchy. It is observed that B1 and B2 textures can be excluded at DUNE for all true δ_{cp} in the upper half plan (UHP, δ_{cp} from 0° to 180°) for any values of θ_{23} at 5σ C.L. If $\theta_{23} = 40.0^\circ$, then DUNE can exclude both B1 and B3 at 5σ irrespective of any true δ_{cp} . For this θ_{23} , DUNE can exclude B2 for all δ_{cp} in the UHP at 5σ . Similarly, for maximal θ_{23} ,

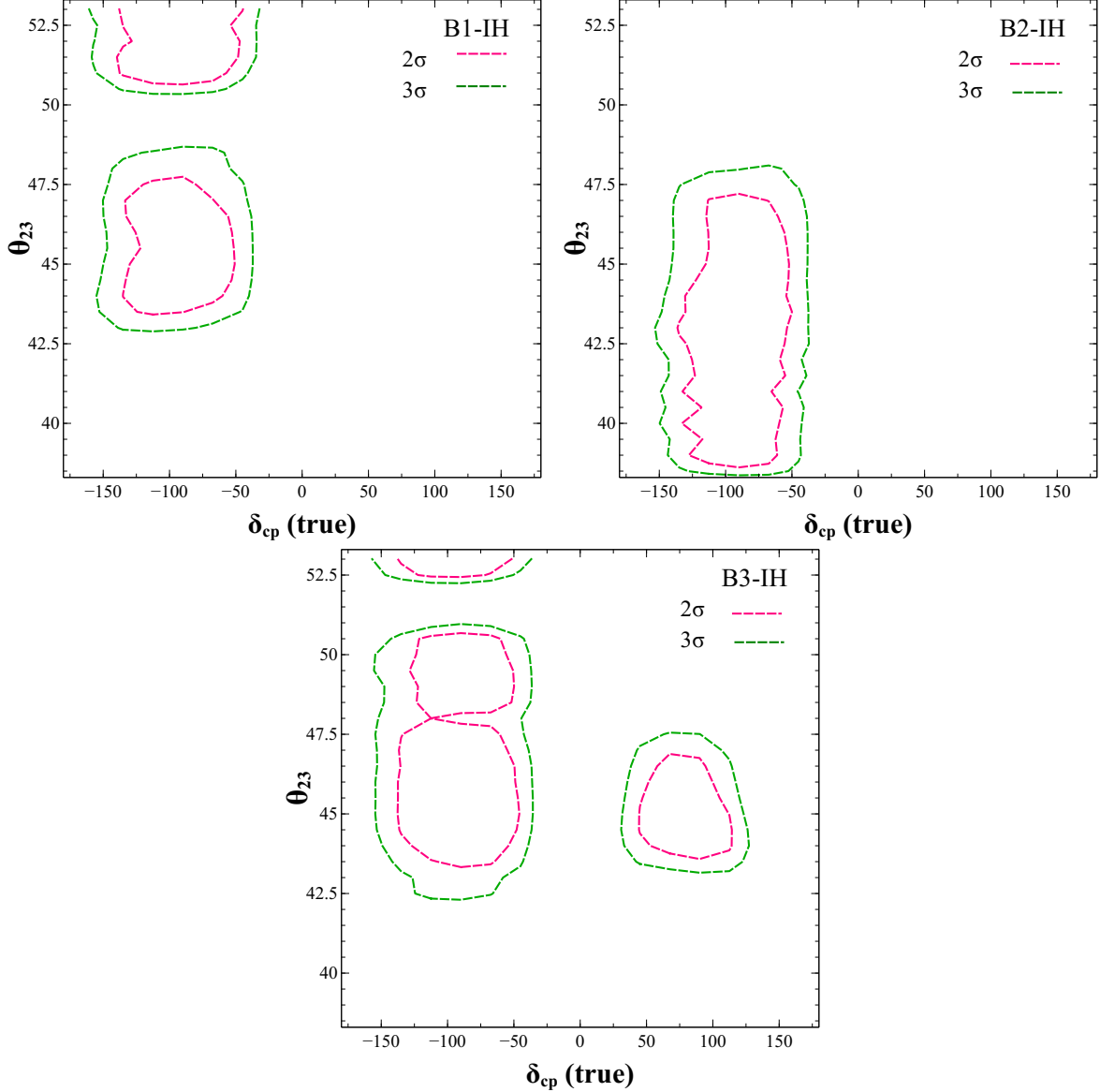


FIG. 19. In the contour plots, we show the allowed regions corresponding to different two-zero textures in IH mode. The green (red) dotted line represents the 3σ (2σ) contour at 1 d.o.f.

both B1 and B2 can be excluded at 5σ in the UHP. If true $\theta_{23} = 50.0^\circ$, then DUNE have the potential to exclude both B1 and B2 at 3σ for all true δ_{cp} and it can rule out B3 at 5σ for all true δ_{cp} in the UHP. We observe from fig. 19 that most of the $\theta_{23} - \delta_{cp}$ parameter space is ruled out at 3σ in case of B1 and B2. All θ_{23} are excluded at 3σ for all true δ_{cp} in the UHP. In the lower half plane of δ_{cp} (LHP, δ_{cp} from -180° to 0°), DUNE can exclude both B1 and B2 at 3σ if $\theta_{23} < 43.0^\circ$ and $\theta_{23} > 48^\circ$ respectively. DUNE can exclude B3 at 3σ for

all true δ_{cp} if Nature chooses θ_{23} such that $\theta_{23} < 42.5^\circ$. DUNE allows B3 almost for all δ_{cp} except some fractions around the CP conserving values. All these textures in IH mode are excluded at DUNE for the CP conserving values at 5σ irrespective of any true θ_{23} .

DUNE is an upcoming experiment and hence it is very much important to ask the following question: if Nature chooses one of these mass texture i.e. the true values of θ_{23} and δ_{cp} lies in the range restricted by the texture, then how DUNE can exclude the present oscillation scenario? To answer that question, we choose the discrete data sets (from fig. 1 to fig. 7) which are an outcome of a constraint equation from the textures, as the ‘data’ or ‘true values’ and in the ‘fit’, we consider the standard oscillation scenario i.e. we vary δ_{cp} and θ_{23} in their 3σ allowed range. Then χ^2 is calculated between ‘data’ and ‘fit’. We show the results (from fig. 20 to fig. 23) as a function of true θ_{23} and true δ_{cp} . If for a particular choice of true parameters, all test values give $\chi^2 > 4$ ($\chi^2 > 9$), then we can say that the standard oscillation scenario can be excluded at 2σ (3σ) C.L. In $\theta_{23} - \delta_{\text{cp}}$ (true) parameter space, a point has been marked by magenta star if for that point χ_{min}^2 is greater than 4 but less than 9. All blue triangles represent the points which give $\chi_{\text{min}}^2 > 9$. So for all coloured points, we can say that DUNE can exclude the standard scenario at 2σ C.L. DUNE can exclude the standard scenario at 3σ C.L. only for the blue points.

VI. CONCLUSIONS

To conclude, in this work, we performed a phenomenological study on one-zero and two-zero textures from DUNE prospective. We first constrain the different possible one-zero and two-zero texture mass matrices from the latest experimental data on oscillation parameters, sum of absolute neutrino mass as well as the lower bound on the half-life of neutrinoless double beta decay. Using the most recent bounds on these parameters, we find that some of the texture zero mass matrices previously shown to be allowed become disfavoured or only marginally allowed. The allowed textures in particular the two-zero texture mass matrices also predict the neutrino parameters like θ_{23} , δ_{cp} etc. to lie in a very specific range that can be probed at long baseline neutrino experiments like the DUNE.

In the second part of our work, we have studied the capability of DUNE to probe different mass textures once it takes data. We have shown our results for both one-zero and two-zero textures for both the hierarchies. Depending on the values of θ_{23} and δ_{cp} that Nature

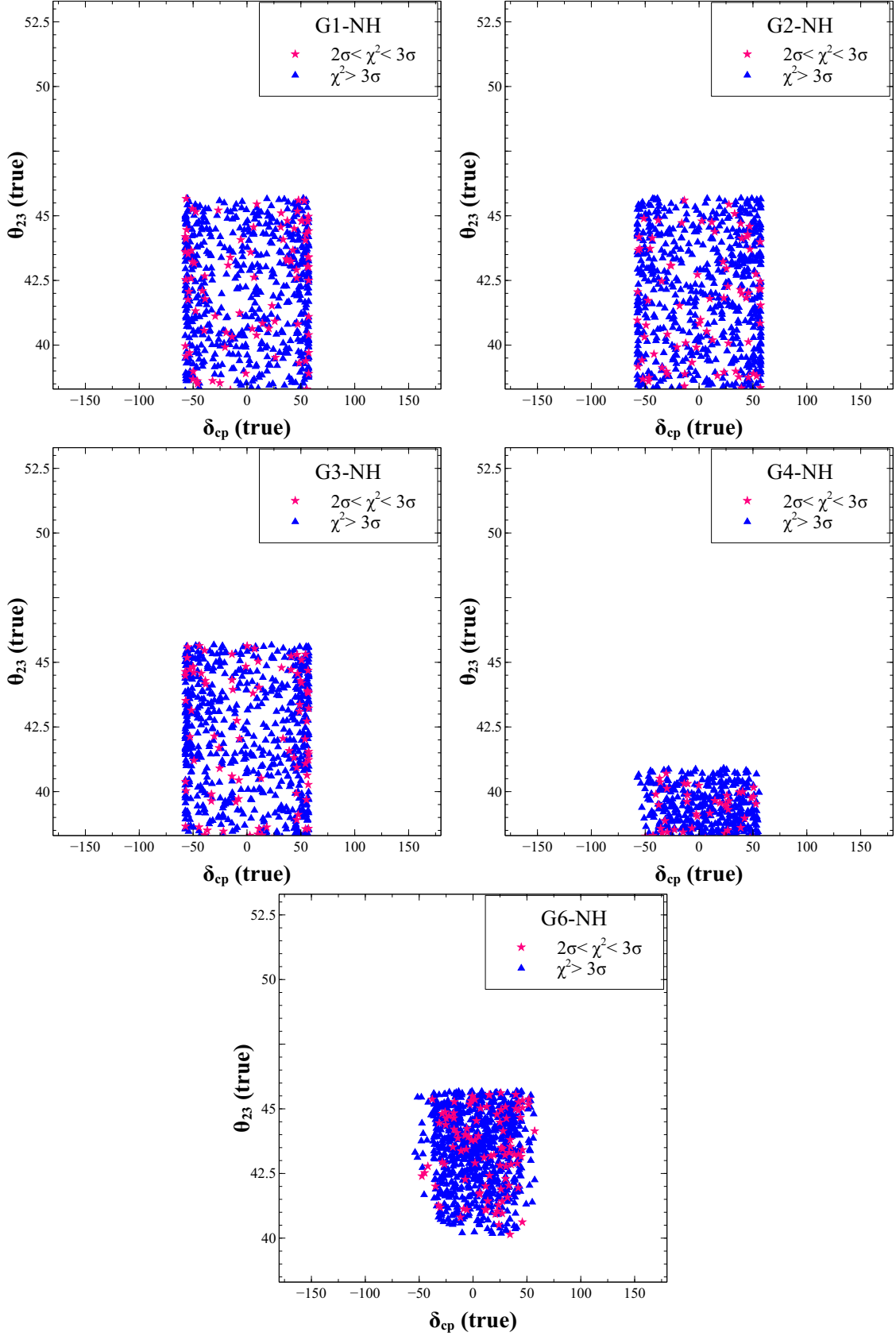


FIG. 20. Region of the $\theta_{23} - \delta_{cp}$ parameter space for which DUNE can establish one-zero texture against the present oscillation scenario for assumed true NH

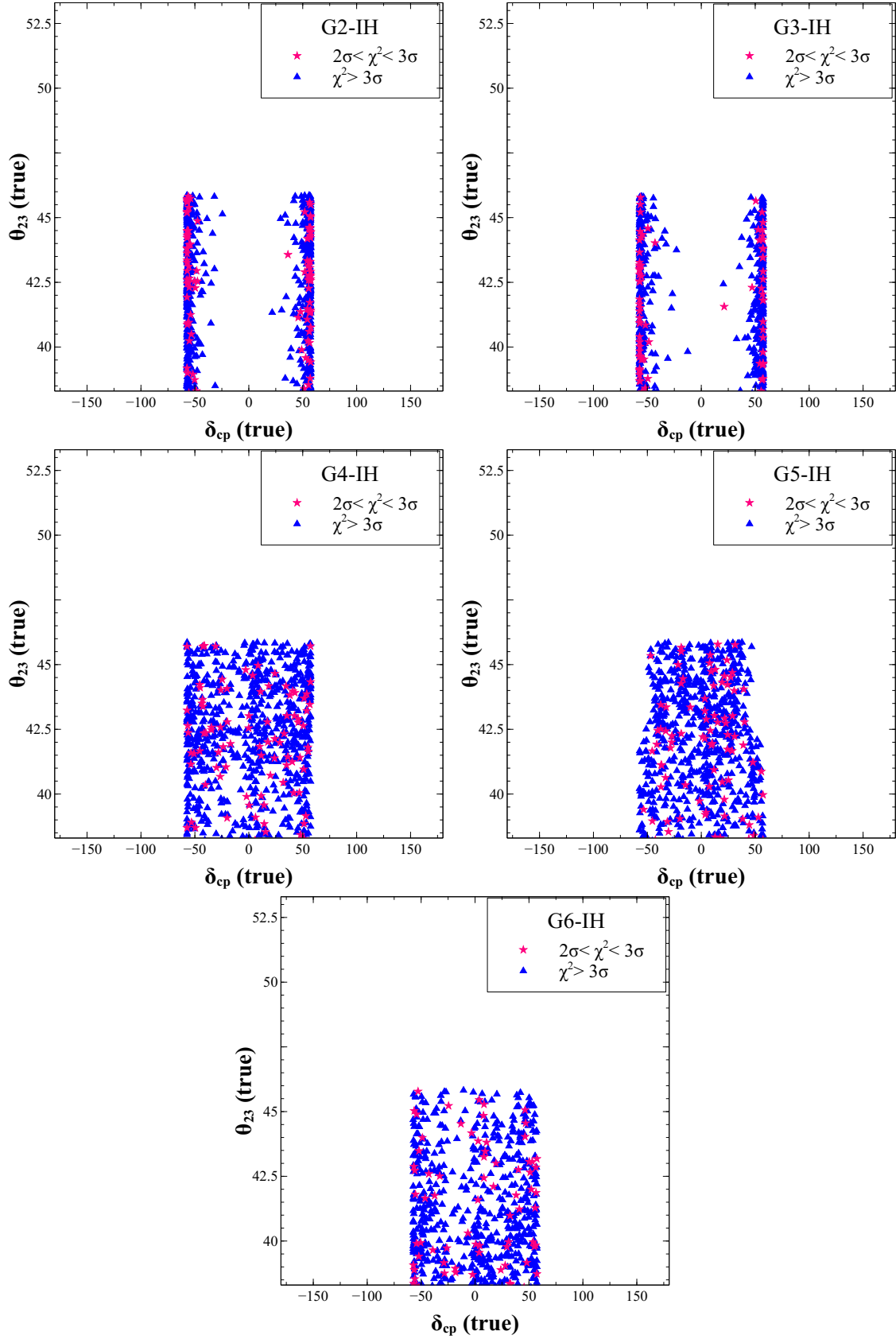


FIG. 21. Region of the $\theta_{23} - \delta_{cp}$ parameter space for which DUNE can establish one-zero texture against the present oscillation scenario for assumed true IH

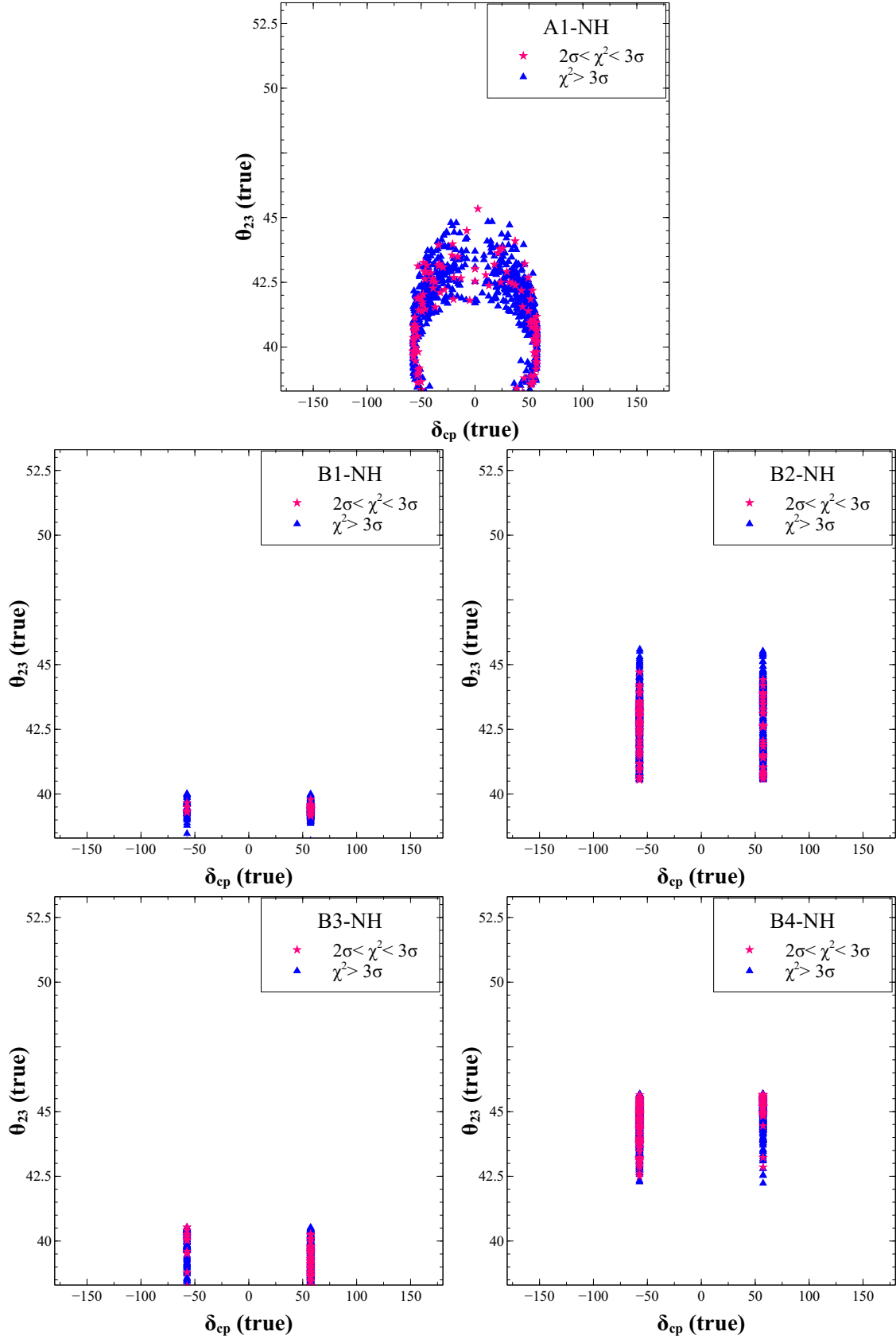


FIG. 22. Region of the $\theta_{23} - \delta_{cp}$ parameter space for which DUNE can establish two-zero texture against the present oscillation scenario for assumed true NH

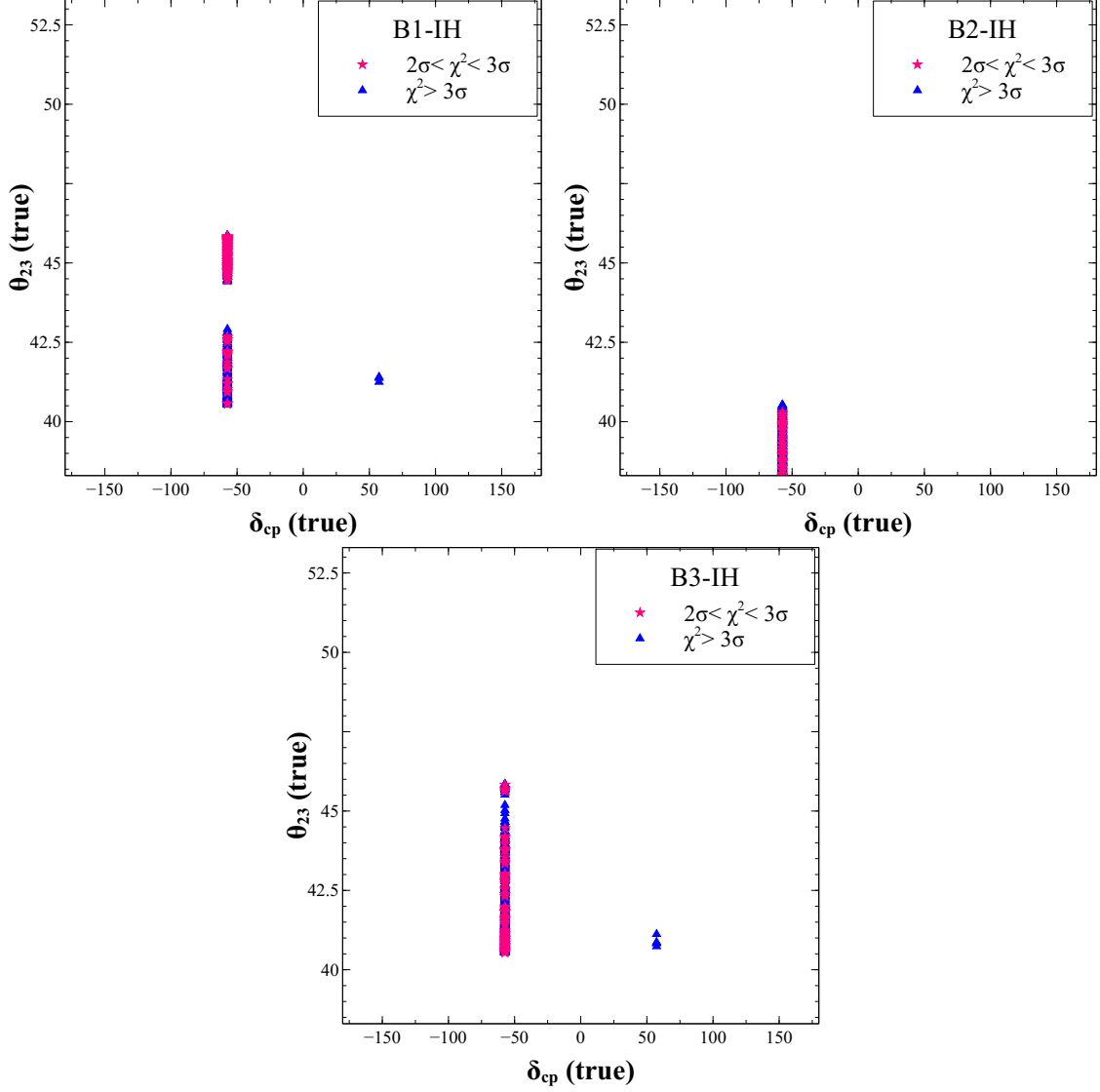


FIG. 23. Region of the $\theta_{23} - \delta_{cp}$ parameter space for which DUNE can establish two-zero texture against the present oscillation scenario for assumed true IH

chooses, how DUNE allows/excludes these textures is presented in this work. From the analyses, we have observed that the most of the $\theta_{23} - \delta_{cp}$ parameter space is allowed for the one-zero textures in both the hierarchies at 3σ . DUNE excludes G4 (G6) texture at 3σ almost for all δ_{cp} if true $\theta_{23} > 47.5^\circ$ ($\theta_{23} < 44^\circ$) and assumed true hierarchy is normal. DUNE can exclude G3 at 3σ for any θ_{23} for all the CP conserving values of δ_{cp} while G4, G5 and G6 are excluded for $\delta_{cp} = \pm\pi$ at 3σ for assumed true IH. Except A1, all other two-zero textures are excluded for CP conserving values at 4σ , irrespective of θ_{23} and hierarchies. We

have observed that these two-zero textures are very interesting from DUNE prospective as most of the true $\theta_{23} - \delta_{\text{cp}}$ parameter space is excluded at DUNE. Specially, for any θ_{23} in the HO, DUNE can exclude B1-NH for all true values of δ_{cp} at 3σ . If θ_{23} is such that $\theta_{23} > 51^\circ$ and $\theta_{23} < 43.5^\circ$, DUNE then can rule out B2-NH for all true δ_{cp} at 3σ C.L.. Similarly, if $\theta_{23} > 48^\circ$ ($\theta_{23} < 44^\circ$), DUNE excludes B3-NH (B4-NH) for all true δ_{cp} at 3σ .

Again, for assumed true IH, we have found that B1 and B2 textures can be excluded at DUNE for all true δ_{cp} in the upper half plan (UHP, δ_{cp} from 0° to 180°) for any values of θ_{23} at 5σ C.L. If Nature chooses θ_{23} such that $\theta_{23} < 43.5^\circ$, DUNE can exclude B3 at 3σ for all true δ_{cp} .

From this study, we have observed that, irrespective of neutrino mass ordering, DUNE can exclude most of the true $\theta_{23} - \delta_{\text{cp}}$ parameter space of B1 texture and hence restricts B1 more tightly.

Since the texture zero mass matrices can be generated by different flavour symmetry models considered in several earlier works [43–52], possible discrimination of different texture zeros at DUNE studied in this work could also disfavour certain flavour symmetry models leading to some particular textures. Although the new physics sector is not directly affecting the neutrino oscillation probabilities analytically, its presence is indirectly tested by probing the specific neutrino parameters it predicts through a particular texture zero mass matrix. This study can also be extended to other texture zero models like the ones with non-diagonal charged lepton mass matrix, the ones with additional light sterile neutrinos. We are working on these possibilities which will be presented in an upcoming work [83].

ACKNOWLEDGMENTS

We acknowledge the use of HRI cluster facility to carry out the computations. DD thanks Prof. Raj Gandhi for his support as well as discussions regarding DUNE. He acknowledges the support from Gauhati University and the DAE Neutrino project at HRI to visit Gauhati University and IIT, Guwahati. He also thanks Suprabh Prakash for some useful discussions during his HRI visit.

Appendix A: Light neutrino mass matrix elements

$$M_{ee} = c_{12}^2 c_{13}^2 m_1 + c_{13}^2 s_{12}^2 m_2 e^{i2\alpha} + s_{13}^2 m_3 e^{i2\beta} \quad (\text{A1})$$

$$M_{e\mu} = M_{\mu e} = c_{13} \left(s_{13} s_{23} m_3 e^{i(\delta_{\text{cp}}+2\beta)} - c_{12} m_1 (c_{23} s_{12} + c_{12} s_{13} s_{23} e^{i\delta_{\text{cp}}}) \right. \\ \left. + s_{12} m_2 e^{i2\alpha} (c_{12} c_{23} - s_{12} s_{13} s_{23} e^{i\delta_{\text{cp}}}) \right) \quad (\text{A2})$$

$$M_{e\tau} = M_{\tau e} = c_{13} \left(c_{23} s_{13} m_3 e^{i(\delta_{\text{cp}}+2\beta)} - s_{12} m_2 e^{i2\alpha} (c_{23} s_{12} s_{13} e^{i\delta_{\text{cp}}} \right. \\ \left. + c_{12} s_{23}) + c_{12} m_1 (-c_{12} c_{23} s_{13} e^{i\delta_{\text{cp}}} + s_{12} s_{23}) \right) \quad (\text{A3})$$

$$M_{\mu\mu} = c_{13}^2 s_{23}^2 m_3 e^{i2(\delta_{\text{cp}}+\beta)} + m_1 (c_{23} s_{12} + c_{12} s_{13} s_{23} e^{i\delta_{\text{cp}}})^2 + m_2 e^{i2\alpha} (c_{12} c_{23} - s_{12} s_{13} s_{23} e^{i\delta_{\text{cp}}})^2 \quad (\text{A4})$$

$$M_{\mu\tau} = M_{\tau\mu} = c_{13}^2 c_{23} s_{23} m_3 e^{i2(\delta_{\text{cp}}+\beta)} + m_1 (c_{12} c_{23} s_{13} e^{i\delta_{\text{cp}}} - s_{12} s_{23}) (c_{23} s_{12} + c_{12} s_{13} s_{23} e^{i\delta_{\text{cp}}}) \\ - m_2 e^{i2\alpha} (c_{23} s_{12} s_{13} e^{i\delta_{\text{cp}}} + c_{12} s_{23}) (c_{12} c_{23} - s_{12} s_{13} s_{23} e^{i\delta_{\text{cp}}}) \quad (\text{A5})$$

$$M_{\tau\tau} = c_{13}^2 c_{23}^2 m_3 e^{i2(\delta_{\text{cp}}+\beta)} + m_2 e^{i2\alpha} (c_{23} s_{12} s_{13} e^{i\delta_{\text{cp}}} + c_{12} s_{23})^2 + m_1 (c_{12} c_{23} s_{13} e^{i\delta_{\text{cp}}} - s_{12} s_{23})^2 \quad (\text{A6})$$

- [1] S. Fukuda et al. (Super-Kamiokande), Phys. Rev. Lett. **86**, 5656 (2001), hep-ex/0103033; Q. R. Ahmad et al. (SNO), Phys. Rev. Lett. **89**, 011301 (2002), nucl-ex/0204008; Phys. Rev. Lett. **89**, 011302 (2002), nucl-ex/0204009; J. N. Bahcall and C. Pena-Garay, New J. Phys. **6**, 63 (2004), hep-ph/0404061; K. Nakamura et al., J. Phys. **G37**, 075021 (2010).
- [2] S. Abe et al. (KamLAND Collaboration), Phys.Rev.Lett. **100**, 221803 (2008).
- [3] K. Abe et al. [T2K Collaboration], Phys. Rev. Lett. **107**, 041801 (2011).
- [4] Y. Abe et al., Phys. Rev. Lett. **108**, 131801 (2012).
- [5] F. P. An et al. [DAYA-BAY Collaboration], Phys. Rev. Lett. **108**, 171803 (2012).
- [6] J. K. Ahn et al. [RENO Collaboration], Phys. Rev. Lett. **108**, 191802 (2012).
- [7] P. Adamson et al. [MINOS Collaboratio], Phys.Rev.Lett. **110**, 171801 (2013).
- [8] I. Esteban, M. C. Gonzalez-Garcia, M. Maltoni, I. Martinez-Soler and T. Schwetz, JHEP **1701**, 087 (2017).
- [9] R. Ade *et al.* [Planck Collaboration], arXiv:1502.01589.

- [10] A. Gando et. al., [KamLAND-Zen Collaboration], Phys. Rev. Lett. **110**, 062502 (2013).
- [11] M. Agostini et. al., [GERDA Collaboration], Phys. Rev. Lett. **111**, 122503 (2013).
- [12] A. Gando et. al., [KamLAND-Zen Collaboration], Phys. Rev. Lett. **117**, 082503 (2016), arXiv:1605.02889.
- [13] M. Agostini et. al., [GERDA Collaboration], Nature **544**, 47 (2017).
- [14] K. Abe et al., [T2K Collaboration], Phys. Rev. **D91**, 072010 (2015).
- [15] K. Abe et al. [T2K Collaboration], Phys.Rev.Lett.112, 181801 (2014),1403.1532.
- [16] P. Adamson et al. [MINOS Collaboration], Phys.Rev.Lett. (2014),1403.0867.
- [17] A. Himmel (Collaboration for the Super-Kamiokande) (2013),1310.6677.
- [18] F. Capozzi, G. Fogli, E. Lisi, A. Marrone, D. Montanino, et al. (2013), 1312.2878.
- [19] P. Vahle (2016), talk given at the Neutrino 2016 Conference, July 4-9, 2016, London, United Kingdom, <http://neutrino2016.iopconfs.org/home>.
- [20] R. Acciarri et al.(DUNE) (2015),1601.05471.
- [21] R. Acciarri et al.(DUNE) (2016),1601.02984.
- [22] T. Alion et al.(DUNE) (2016),1606.09550.
- [23] C. Adams et al. (LBNE) (2013), 1307.7335, URL <http://www.osti.gov/scitech/biblio/1128102>.
- [24] D. Ayres et al. (NOÏA Collaboration) (2004), hep-ex/0503053.
- [25] R. Patterson, Talk given at the Neutrino 2012 Conference, June 3-9, 2012, Kyoto, Japan, URL: <http://neu2012.kek.jp/>.
- [26] S. K. Agarwalla, S. Prakash, S. Uma Sankar, JHEP**03** (2014) 087, 1304.3251.
- [27] V. Barger, A. Bhattacharya, A. Chatterjee, R. Gandhi, D. Marfatia, M. Masud, Phys. Rev. D **89**, 011302 (2014), 1307.2519.
- [28] N. Nath, M. Ghosh, S. Goswami, (2015), 1511.07496.
- [29] K. Bora, D. Dutta, P. Ghoshal, Mod.Phys.Lett.A **30**, 1550066 (2015), 1405.7482.
- [30] K. Bora, D. Dutta, J. of Physics, Conf. series (IOP UK), vol 481, p 012019, 2014, 1209.1870.
- [31] G. L. Fogli and E. Lisi, Phys. Rev.D**54**, 3667 (1996),[hep-ph/9604415].
- [32] K. Hiraideet al., Phys.Rev.D**73**, 093008 (2006), [hep-ph/0601258].
- [33] C.R. Das, J. Maalampi, J. Pulido, S. Vihonen, (2016), 1606.02504.
- [34] R. Gandhi, P. Ghoshal, S. Goswami, P. Mehta, S. Uma Sankar, Phys.Rev. D**73** (2006) 053001, hep-ph/0411252.

- [35] T. Lee, Phys.Rev. **D8**, 1226 (1973).
- [36] T. Lee, Phys.Rept. 9, 143 (1974).
- [37] V. Barger, A. Bhattacharya, A. Chatterjee, R. Gandhi, D. Marfatia, M. Masud, Int.J.Mod.Phys. A31, 1650020 (2016),1405.1054.
- [38] S. Prakash, S. K. Raut, S. Uma Sankar, Phys.Rev. D86 (2012) 033012, 1201.6485.
- [39] S. Kumar Agarwalla, S. Prakash, S. Uma Sankar, JHEP 1403 (2014) 087, 1304.3251.
- [40] D.Dutta, K. Bora, Mod.Phys.Lett.A 30, 1550017 (2015), 1409.8248.
- [41] K. Bora, G. Ghosh, D. Dutta, Adv.High Energy Phys. 2016 (2016) 9496758, 1606.00554.
- [42] P. O. Ludl and W. Grimus, JHEP **1407**, 090 (2014).
- [43] M. Berger and K. Siyeon, Phys. Rev. **D64**, 053006 (2001).
- [44] C. I. Low, Phys. Rev. **D70**, 073013 (2004).
- [45] C. I. Low, Phys. Rev. **D71**, 073007 (2005).
- [46] W. Grimus, A. S. Joshipura, L. Lavoura and M. Tanimoto, Eur. Phys. J. **C36**, 227 (2004).
- [47] Z. -z. Xing and S. Zhou, Phys. Lett. **B679**, 249 (2009).
- [48] S. Dev, S. Gupta and R. R. Gautam, Phys. Lett. **B701**, 605 (2011).
- [49] T. Araki, J. Heeck and J. Kubo, JHEP **1207**, 083 (2012).
- [50] R. G. Felipe and H. Serodio, Nucl. Phys. **B886**, 75 (2014).
- [51] A. Dighe and N. Sahu, arXiv:0812.0695.
- [52] W. Grimus and L. Lavoura, J. Phys. **G31**, 693 (2005).
- [53] Z. -z. Xing, Phys. Rev. **D69**, 013006 (2004).
- [54] E. Lashin and N. Chamoun, Phys. Rev. **D85**, 113011 (2012).
- [55] K. Deepthi, S. Gollu and R. Mohanta, Eur. Phys. J. **C72**, 1888 (2012).
- [56] R. R. Gautam, M. Singh and M. Gupta, Phys. Rev. **D92**, 013006 (2015).
- [57] L. M. Cebola, D. E. Costa and R. G. Felipe, Phys. Rev. **D92**, 025005 (2015).
- [58] P. H. Frampton, S. L. Glashow and D. Marfatia, Phys. Lett. **B536**, 79 (2002).
- [59] Z. -z. Xing, Phys. Lett. **B530**, 159 (2002).
- [60] Z. -z. Xing, Phys. Lett. **B539**, 85 (2002).
- [61] A. Kageyama, S. Kaneko, N. Shimoyana and M. Tanimoto, Phys. Lett. **B538**, 96 (2002).
- [62] S. Dev, S. Kumar, S. Verma and S. Gupta, Phys. Rev. **D76**, 013002 (2007).
- [63] P. Ludle, S. Morisi and E. Peinado, Nucl. Phys. **B857**, 411 (2012).
- [64] S. Kumar, Phys. Rev. **D84**, 077301 (2011).

- [65] H. Fritzsch, Z. -z. Xing and S. Zhou, JHEP **1109**, 083 (2011).
- [66] D. Meloni and G. Blankenburg, Nucl. Phys. **B867**, 749 (2013).
- [67] D. Meloni, A. Meroni and E. Peinado, Phys. Rev. **D89**, 053009 (2014).
- [68] S. Dev, R. R. Gautam, L. Singh and M. Gupta, Phys. Rev. **D90**, 013021 (2014).
- [69] S. Dev, L. Singh and D. Raj, Eur. Phys. J. **C75**, 394 (2015).
- [70] M. Borah, D. Borah and M. K. Das, Phys. Rev. **D91**, 113008 (2015).
- [71] S. Kaneko and M. Tanimoto, Phys. Lett. **B551**, 127 (2003).
- [72] S. Kaneko, M. Katsumata and M. Tanimoto, JHEP **0307**, 025 (2003).
- [73] S. Dev and S. Verma, Mod. Phys. Lett. **A25**, 2837 (2010).
- [74] M. Bando, S. Kaneko, M. Obara and M. Tanimoto, Prog. Theor. Phys. **112**, 533 (2004).
- [75] T. P. Nguyen, Mod. Phys. Lett. **A29**, 1450038 (2014).
- [76] R. Kalita and D. Borah, Int. J. Mod. Phys. **A31**, 1650008 (2016).
- [77] P. Huber, M. Lindner, and W. Winter, Comput.Phys.Commun. **167**, 195 (2005), hep-ph/0407333.
- [78] P. Huber, J. Kopp, M. Lindner, M. Rolinec, and W. Winter, Comput. Phys. Commun. **177**, 432 (2007), hep-ph/0701187.
- [79] Z.-z. Xing, pp. 442–449 (2004), hep-ph/0406049.
- [80] Jon Urheim, Talk given at the Neutrino 2016 Conference, July 4-9, 2016, South Kensington, Landon URL: <http://neutrino2016.iopconfs.org/programme>.
- [81] R. Acciarri et al.[DUNE collaboration], (2016), 1601.05471.
- [82] W. Rodejohann, Int. J. Mod. Phys. **E20**, 1833 (2011).
- [83] K. Bora, D. Borah and D. Dutta, *In preparation*.